

8524

CONTRACTOR REPORT

SAND89-7051
Unlimited Release
UC-261

RS-8232-2/069848

c.1

Measurements of Surface Pressures on an Operating Vertical-Axis Wind Turbine



8232-2/069848



0000001 -

Robert E. Akins
Washington and Lee University
Lexington, VA 24450

Prepared by Sandia National Laboratories Albuquerque, New Mexico 87185
and Livermore, California 94550 for the United States Department of Energy
under Contract DE-AC04-76DP00789

Printed November 1989

Issued by Sandia National Laboratories, operated for the United States Department of Energy by Sandia Corporation.

NOTICE: This report was prepared as an account of work sponsored by an agency of the United States Government. Neither the United States Government nor any agency thereof, nor any of their employees, nor any of their contractors, subcontractors, or their employees, makes any warranty, express or implied, or assumes any legal liability or responsibility for the accuracy, completeness, or usefulness of any information, apparatus, product, or process disclosed, or represents that its use would not infringe privately owned rights. Reference herein to any specific commercial product, process, or service by trade name, trademark, manufacturer, or otherwise, does not necessarily constitute or imply its endorsement, recommendation, or favoring by the United States Government, any agency thereof or any of their contractors or subcontractors. The views and opinions expressed herein do not necessarily state or reflect those of the United States Government, any agency thereof or any of their contractors.

Printed in the United States of America. This report has been reproduced directly from the best available copy.

Available to DOE and DOE contractors from
Office of Scientific and Technical Information
PO Box 62
Oak Ridge, TN 37831

Prices available from (615) 576-8401, FTS 626-8401

Available to the public from
National Technical Information Service
US Department of Commerce
5285 Port Royal Rd
Springfield, VA 22161

NTIS price codes
Printed copy: A05
Microfiche copy: A01

SAND89-7051
Unlimited Release
Printed November 1989

**MEASUREMENTS OF SURFACE PRESSURES ON AN
OPERATING VERTICAL-AXIS WIND TURBINE**

Robert E. Akins
Washington and Lee University
Lexington, VA 24450

Sandia Contract: 23-0836

ABSTRACT

This report describes measurements of surface pressures on a vertical-axis wind turbine using pressure transducers mounted at the equator of one blade of the rotor. These pressure transducers were monitored as a function of relative rotor position and incident wind speed to obtain the distribution of surface pressure. The measured pressure distributions are substantially different from wind-tunnel results. The surface pressures were integrated to obtain tangential and normal force coefficients as a function of rotor position relative to the incident wind. These measured force coefficients are compared with wind-tunnel results for tip-speed ratios from 2.20 to 4.60. At low tip-speed ratios there is evidence of dynamic stall for the upwind portion of the rotation.

ACKNOWLEDGMENTS

Many individuals were involved in the early aspects of this project. Robert Croll, Don McBride, and Dave Powers of the Experimental Aerodynamics Division, SNLA, planned most of the instrumentation and were involved with the calibration of the flow-angularity probe. Paul Klimas of the Wind Energy Research Division, SNLA, was involved in the project from its inception in the planning and execution of the experiment and in the interpretation of the results. Gerry McNerny of US Windpower (formerly a contractor for Sandia) worked with the initial data reduction algorithms. Jack Cyrus, Mark Worstell, and Emil Kadlec of the Wind Energy Research Division SNLA were always willing to help with data acquisition under often adverse conditions.

Washington and Lee University has provided computer time for much of the data analysis and graphics associated with this final report. Al Eggers and Lloyd Jones of RANN have carefully followed the data reduction phase of this project, have asked many helpful questions, and have therefore contributed to this report.

TABLE OF CONTENTS

Abstract	iii
Acknowledgments	iv
Table of Contents	v
List of Tables	vi
List of Figures	vii
1. Introduction	1
2. Experiment and Data Acquisition	3
2.1 Turbine Configuration	3
2.2 Instruments	3
2.3 Installation	5
2.4 Calibration	6
2.5 Data Acquisition	7
3. Data Reduction	9
3.1 Adjustments to Measured Data	9
3.1.1 Pressure Transducers	9
3.1.2 Rotor Position Indicator	9
3.1.3 Reference Wind Speed	10
3.1.4 Density Corrections	10
3.2 Sign Conventions, Coordinate System, and Coefficient Definitions	11
3.3 Bins Approach	12
3.4 Fits to Data	15
3.5 CT/CN Calculation	15
3.6 Angle of Attack	16
4. Results	17
4.1 Pressure Coefficients	17
4.2 Force Coefficients	23
5. Conclusions	29

LIST OF TABLES

1. Pressure transducer locations on the inner and outer surface of blade (as a fraction of chord).	34
2. Transducer locations used in the data analysis.	34
3. CN and CT for Tip-speed ratio 2.20.	35
4. CN and CT for Tip-speed ratio 2.33.	36
5. CN and CT for Tip-speed ratio 2.49.	37
6. CN and CT for Tip-speed ratio 2.66.	38
7. CN and CT for Tip-speed ratio 2.86.	39
8. CN and CT for Tip-speed ratio 3.09.	40
9. CN and CT for Tip-speed ratio 3.70.	41
10. CN and CT for Tip-speed ratio 4.60.	42

LIST OF FIGURES

1. Sandia/DOE Research Turbine, Albuquerque, NM.	43
2. Flow-Angularity Probe used in the Test Program.	43
3. Pressure Transducer Mounting Arrangement.	44
4. Pressure Transducers Installed on Turbine.	44
5. Nomenclature used in Defining Relative Rotor Position.	45
6. Sign Convention used with Force Coefficients.	45
7a. Variation in Pressure Coefficients Single Record: $x/c = 0.00$, Tip-speed ratio 7.98.	46
7b. Variation in Pressure Coefficients Single Record: $x/c = 0.00$, Tip-speed ratio 3.23.	46
7c. Variation in Pressure Coefficients Single Record: $x/c = 0.05$, Tip-speed ratio 7.98.	47
7d. Variation in Pressure Coefficients Single Record: $x/c = 0.05$, Tip-speed ratio 3.23.	47
8a. Variation in Pressure Coefficients Combined Record: $x/c = 0.00$, Tip-speed ratio 3.09.	48
8b. Variation in Pressure Coefficients Combined Record: $x/c = 0.05$, Tip-speed ratio 3.09.	48
9. Example of Curve Fit, Pressure Distributions.	49
10a. Pressure Distribution Outer Surface: Angle of Attack 6 Degrees.	50
10b. Pressure Distribution Inner Surface: Angle of Attack 6 Degrees.	50
11a. Pressure Distribution Outer Surface: Angle of Attack 8 Degrees.	51
11b. Pressure Distribution Inner Surface: Angle of Attack 8 Degrees.	51
12a. Pressure Distribution Outer Surface: Angle of Attack 12 Degrees.	52
12b. Pressure Distribution Inner Surface: Angle of Attack 12 Degrees.	52
13a. Pressure Coefficients as a Function of Relative Rotor Position: Outer Surface, Tip-speed ratio 2.33.	53
13b. Pressure Coefficients as a Function of Relative Rotor Position: Inner Surface, Tip-speed ratio 2.33.	53
14a. Pressure Coefficients as a Function of Relative Rotor Position: Outer Surface, Tip-speed ratio 3.09.	54
14b. Pressure Coefficients as a Function of Relative Rotor Position: Inner Surface, Tip-speed ratio 3.09.	54
15a. Pressure Coefficients as a Function of Relative Rotor Position: Outer Surface, Tip-speed ratio 4.60.	55
15b. Pressure Coefficients as a Function of Relative Rotor Position: Inner Surface, Tip-speed ratio 4.60.	55
16a. Pressure Coefficients as a Function of Relative Rotor Position: Outer Surface, Tip-speed ratio 8.92.	56
16b. Pressure Coefficients as a Function of Relative Rotor Position: Inner Surface, Tip-speed ratio 8.92.	56

17a. Surface Plot Pressure Coefficients: Outer Surface, Tip-speed ratio 2.33.	57
17b. Surface Plot Pressure Coefficients: Inner Surface, Tip-speed ratio 2.33.	58
17c. Surface Plot Pressure Coefficients: Net Force, Tip-speed ratio 2.33.	59
18a. Surface Plot Pressure Coefficients: Outer Surface, Tip-speed ratio 3.09.	60
18b. Surface Plot Pressure Coefficients: Inner Surface, Tip-speed ratio 3.09.	61
18c. Surface Plot Pressure Coefficients: Net Force, Tip-speed ratio 3.09.	62
19a. Surface Plot Pressure Coefficients: Outer Surface, Tip-speed ratio 4.60.	63
19b. Surface Plot Pressure Coefficients: Inner Surface, Tip-speed ratio 4.60.	64
19c. Surface Plot Pressure Coefficients: Net Force, Tip-speed ratio 4.60.	65
20a. Surface Plot Pressure Coefficients: Outer Surface, Tip-speed ratio 8.92.	66
20b. Surface Plot Pressure Coefficients: Inner Surface, Tip-speed ratio 8.92.	67
20c. Surface Plot Pressure Coefficients: Net Force, Tip-speed ratio 8.92.	68
21. Normal Force Coefficients: Tip-speed ratio 2.20.	69
22. Normal Force Coefficients: Tip-speed ratio 2.33.	69
23. Normal Force Coefficients: Tip-speed ratio 2.49.	70
24. Normal Force Coefficients: Tip-speed ratio 2.66.	70
25. Normal Force Coefficients: Tip-speed ratio 2.86.	71
26. Normal Force Coefficients: Tip-speed ratio 3.09.	71
27. Normal Force Coefficients: Tip-speed ratio 3.70.	72
28. Normal Force Coefficients: Tip-speed ratio 4.60.	72
29. Tangential Force Coefficients: Tip-speed ratio 2.20.	73
30. Tangential Force Coefficients: Tip-speed ratio 2.33.	73
31. Tangential Force Coefficients: Tip-speed ratio 2.49.	74
32. Tangential Force Coefficients: Tip-speed ratio 2.66.	74
33. Tangential Force Coefficients: Tip-speed ratio 2.86.	75
34. Tangential Force Coefficients: Tip-speed ratio 3.09.	75
35. Tangential Force Coefficients: Tip-speed ratio 3.70.	76
36. Tangential Force Coefficients: Tip-speed ratio 4.60.	76

1. INTRODUCTION

The ability to understand and accurately predict the aerodynamic forces acting on a wind turbine is an essential step in the design process. These forces affect both the power production of the turbine and the structural response of the rotor. Existing techniques for predicting aerodynamic performance and structural loads utilize two-dimensional airfoil section properties and an empirical model to include effects of dynamic stall. Prior efforts to validate these models have in all cases been based on the measurement of either a torque or a stress integrated over the entire turbine. The local pressures or forces acting on the blade of the wind turbine have not previously been investigated and will be of value in future model validation.

An experimental program was designed and implemented to measure the surface pressures at a single location on a wind turbine. This program not only considered the pressure distribution at a single location on the rotor, but also the local forces obtained by integrating the pressures, and the variation of these forces as a function of rotor position and incident wind speed. Pressure transducers were installed in one blade of the DOE/Sandia 17M Darrieus vertical-axis wind turbine (VAWT). The transducers were distributed along the chord of the blade at the equator of the turbine. Additional instrumentation was used to measure the incident flow field and the rotor position relative to the incident wind. These measurements were

limited to a single rotor configuration and a single operating speed. The measurements will be used to verify existing aerodynamic models, to improve these models, and to provide guidance for future experiments and research.

This report summarizes the experimental setup, the data acquisition and analysis, and the results of the study. Many problems were encountered during the program and the results discussed are of more qualitative than quantitative value.

2. EXPERIMENT AND DATA ACQUISITION

2.1 Turbine Configuration

Measurements were obtained using the DOE/Sandia 17M research VAWT located at Sandia National Laboratories, Albuquerque, NM. The turbine used in this program, shown in Figure 1, has two blades and a height-to-diameter ratio of 1.0. The blades have NACA 0015 cross section with a chord of 0.612 m (2.0 ft) and are attached to the tower at the roots only; no struts are used in this particular design. The blades were bent to a straightline-circular arc-straightline troposkein approximation from a single extrusion and there were no blade-to-blade joints. Rotor radius is 8.36 m (27.3 ft), ground clearance is 4.88 m (10.0 ft), and swept area of the turbine is 187 m² (2000 ft²). Further details about the turbine are contained in Reference 1. The turbine operated at 38.7 rpm and 50.6 rpm for these tests, but only the results for 38.7 rpm are presented. Several key pressure transducers were inoperative at 50.6 rpm and there were not enough data to define the pressure distribution and associated forces.

2.2 Instruments

Flush-mounted pressure transducers were used to measure the surface pressures. These transducers were selected based on several criteria: adequate frequency response, minimal mechanical impact on the blade, insensitivity to acceleration and temperature, ability to measure very small pressures, ruggedness and weather resistance, and relatively small size to allow dense

placement at a given spanwise location on the blade. Entran Model EPF 200-10 piezoresistive transducers were selected as the most appropriate choice available in late 1980. The transducers had a sealed reference pressure and as such were neither absolute nor differential. The sealed reference pressure was constant and by electrically adjusting the reading to zero just prior to a test, the transducers were used in a differential manner with the reference pressure equal to ambient atmospheric. The zero reading was sensitive to ambient temperature and changes in atmospheric pressure. Anticipated pressures were at most 1% of 10 psi full scale and therefore the transducers were used with amplifiers and were very sensitive to zero shift. The transducers have a circular sensing surface with a diameter of 5mm (0.2 in). They were mounted in small machined recesses in the blade as described in section 2.3.

Incident wind speed and direction were measured with a cup-vane anemometer system mounted on a tower extending from the top of the turbine along the axis of rotation. This installation arrangement was used in all past performance measurements for this turbine and the readings were not influenced by the operation of the wind turbine (2). The anemometer was a Teledyne Geotech Model 1564B with a distance constant of 1.5 m (5 ft) of air. The corresponding vane was a Teledyne Geotech Model 1656B with a distance constant of 0.5 m (1.6 ft) of air and a damping ratio of 0.2 at a 10 degree initial angle of attack.

The rotor position was monitored with a synchro system

attached to the base of the rotor with a chain drive. A flow-angularity probe to measure local incident wind speed, angle of attack and yaw angle was mounted on the blade. The layout of this probe is shown in Figure 2. The details of the installation and calibration of the probe are described in Sections 2.3 and 2.4.

A 64 channel PCM (pulsed code modulator) system was used to collect and transmit data from the rotating reference frame associated with the turbine to the ground. All analog signals were amplified as necessary and digitized using the PCM located on the rotor. A high-level digital pulse stream was sent via slip rings to the ground-based data acquisition system. Important ground-based signals such as rotor position and incident wind speed and direction were fed from the ground through the slip rings to the PCM so that all signals were digitized simultaneously. This arrangement allowed multiple channels of low-level signals to be amplified and passed through a single set of slip rings. A common amplifier was used in the PCM at a nominal gain of 2000 for the pressure signals. Other signals in the data stream did not require amplification. The analog-to-digital conversion of the PCM was at a fixed rate of 50 samples per second. The digital pulse stream was sent to a computer and stored on disk in real time.

2.3 Installation

A wind-tunnel test was conducted to verify the installation and operation of the pressure transducers in a prototype section

of blade. In analyzing the results from this test, it was found that for the small pressures observed during wind turbine operation, convective cooling of the transducer diaphragm caused significant errors. In order to alleviate this problem, a system was devised which would thermally insulate the transducers from this effect. Each transducer was placed in a separate mounting device and immersed in silicone to provide insulation prior to mounting in the blade. This mounting system reduced the frequency response of the transducers, but the measured frequency response was still greater than 50 hz. The sample rate of the PCM system set the upper limit of frequency response for the entire system at 25 hz. The devices containing the transducers were mounted in milled locations in the blade and covered with a thin sheet of Mylar with holes over the transducers. The Mylar was used to provide protection for the transducers from both dust and moisture. The arrangement is shown in Figure 3. This method of mounting provided adequate thermal insulation, was relatively easy to install, and provided some protection for the transducers from moisture and dust. The pressure transducers were located a distance of 0.25 of the chord below the equator of the turbine. The locations of the pressure transducers are listed in Table 1.

The flow-angularity probe was mounted on the leading edge of the airfoil a distance of 0.25 of the chord above the equator. The tip of the probe was 21.6 cm (8.5 in) in front of the leading edge of the blade. Figure 4 shows the installation of both the

flow-angularity probe and the transducers in the blade of the turbine.

2.4 Calibration

The pressure transducers were calibrated in a laboratory environment prior to mounting in the blade. It was not possible to provide a known reference pressure to the blade and the transducers could therefore not be calibrated in place. The pre-test calibration was used for the duration of the test program, approximately 3 months. The common amplifier used with all of the pressure channels was electrically calibrated in place on the rotor.

The flow-angularity probe was calibrated in an extensive wind-tunnel test. The probe calibration took into account effects due to angle of attack and interference caused by the blade. The differential taps used to measure angle of attack and yaw angle were also calibrated in the wind-tunnel test. The measured results for angle of attack and yaw angle proved to be unreliable in the test program, probably due to the unsteady conditions. In the data reduction, only the measurement of the local wind speed incident to the blade was used to calculate pressure coefficients. All angles of attack were computed as outlined in section 3.6.

2.5 Data Acquisition

The turbine was operated at 38.7 rpm over a two month period from March to April 1982. Data were collected on all channels simultaneously at 50 samples per second, corresponding to 77

samples per revolution of the rotor. Record length was 12 minutes, limited by the capacity of the disk storage. Data were obtained at wind speeds spanning the entire range of operation of the turbine.

Prior to and after each test segment, the zero readings of the pressure transducers were checked. A bucket truck was used to gain access to the blade and a foam cuff was placed over the instrumented portion of the blade. This cuff damped any effects due to the wind and exposed each transducer to ambient atmospheric pressure. Readings with the cuff in place were taken using the data acquisition system. Zero readings were corrected prior to each test run (the data acquisition system stored both a calibration factor and a zero for each channel). Post-run zero readings were compared with the pre-run readings. If a shift of greater than 5% of anticipated maximum pressure occurred during a run, the readings from that transducer were not used. Smaller changes were corrected in the data reduction to the average of the pre- and post-run values. In most instances the zero readings did not change substantially from run to run on a given day.

The stored data files include a header with calibration factors and zero values for each channel and blocks of data for each sample time. The blocks consist of readings for each of the 64 channels of the PCM system. A 12 minute run consists of over 2 million numbers.

3. DATA REDUCTION

3.1 Adjustments to Measured Data

3.1.1 Pressure Transducers

The average of the zero readings of the pressure transducers taken before and after each run was used to adjust the raw data prior to analysis. This modification was only made if the two values differed by less than 5% maximum absolute value of pressure expected in the run. When larger shifts were observed, the data were discarded.

3.1.2 Rotor Position Indicator

One of the key independent variables in the experiment was the rotor position relative to the incident wind. The synchro system provided a continuous analog indication of the absolute rotor position. Two major problems occurred which required corrections to the raw data. The synchro provided a sawtooth signal which reset each revolution, but the interval required for the signal to reset was greater than the sample interval. This difficulty caused several samples of rotor position to be in error each rotation. The data reduction algorithm searched for the reset of the synchro, forced the sawtooth to occur within a single time step, and checked to insure the correction did not alter the period of the turbine.

A more significant problem was caused by slipping of the synchro relative to the rotor. This problem was caused by a chain jumping from a sprocket and was not apparent until after the test program was completed. To salvage as much data as possible, a

correction based on the angle of attack measured with the flow-angularity probe was developed. The sign of the angle of attack changed when the blade was in an upwind position, a relative rotor position of 0 degrees. Using this fact and the instantaneous reading of wind direction from the top of the turbine, a correction to the zero reading of the rotor position indicator was computed each rotation of the turbine. The routine was checked on some of the earlier runs where the synchro was operating properly and found to be accurate. A record of the correction for each run was examined, and if any anomalous behavior was noted, the record was not included in the composite data reduction.

3.1.3 Reference Wind Speed

Prior to any data reduction, the reference wind speed was corrected from the reference height to the turbine centerline using the average wind shear measured at the test location (3). A power-law exponent of 0.1 was used and the measured wind speed was reduced by a factor of 0.91. Because the reference anemometer was located directly above the rotor, no corrections for lack of spatial correlation were applied.

3.1.4 Density Corrections

All pressure measurements were divided by the incident dynamic pressure measured with the flow-angularity probe at each time step to obtain a pressure coefficient. All subsequent data reduction was in terms of the pressure coefficients and was independent of any density effects. Therefore, no corrections

were made to any of the measured data for density effects.

3.2 Sign Conventions, Coordinate System, and Coefficient Definitions

A key independent variable in the data reduction and interpretation is the rotor position relative to the incoming wind as defined in Figure 5. The relative rotor position is a function of both the absolute rotor position and the incident wind direction measured above the turbine. Both of these quantities change as a function of time. A relative rotor position of 0 degrees corresponds to the instrumented blade heading directly into the incident wind. Relative rotor positions from 0 to 180 degrees correspond to the upwind half of the rotation of the rotor and 180 to 360 degrees correspond to the downwind half of the rotation.

Pressure coefficients are defined by the following equation:

$$C_P = \frac{(P - P_o)}{0.5\rho V^2} \quad (1)$$

where:

C_P = pressure coefficient
 P = absolute pressure measured on blade
 P_o = ambient static pressure
 ρ = density of ambient air
 V = incident wind speed measured at blade .

A positive pressure coefficient corresponds to a stagnation region or pressure greater than atmospheric. A pressure coefficient of zero corresponds to ambient atmospheric pressure.

The sign convention for the normal force coefficient, C_N , and the tangential force coefficient, C_T , is shown in Figure 6. C_N is positive toward the center of rotation of the turbine and C_T

is positive in the direction of rotation. The angle of attack is defined as positive when the resultant incident wind is coming from outside of the rotor. Angles of attack and CN will be positive for relative rotor positions from 0 to 180 degrees.

CN and CT are defined as:

$$CN = \frac{FN}{0.5\rho V^2 C} \quad (2)$$

where:

CN = normal force coefficient
FN = normal force/unit span
 ρ = density of ambient air
V = incident wind speed measured at blade
C = blade chord.

$$CT = \frac{FT}{0.5\rho V^2 C} \quad (3)$$

where:

CT = tangential force coefficient
FT = tangential force/unit span
 ρ = density of ambient air
V = incident wind speed measured at blade
C = chord of blade.

3.3 Bins Approach

Based on past experience with measurements on operating wind turbines, a data reduction technique based on the method of bins was used. Several references explain the method of bins and variations (4,5,6). The data reduction scheme treated the local surface pressure as the dependent variable and the incident wind speed and the relative rotor position as the independent variables. The instantaneous values of pressure for a given wind speed and relative rotor position only repeat in an average sense. A statistical combination of the data was considered from the outset of the test program and a two-dimensional application

of the method of bins was employed. In performance measurements, the output torque is measured as a function of wind speed only, a one-dimensional application of the method of bins.

The surface pressures were divided by the dynamic pressure measured with the flow-angularity probe as the first step in the data reduction. This normalization was done at each time step before any sorting as a function of wind speed or relative rotor position. At this point the pressures were all in terms of a pressure coefficient as defined by equation 1. The measured pressure coefficients for each location were separated as a function of instantaneous wind speed (corrected for shear) in 0.447 m/s (1.0 mph) increments and relative rotor position in 6 degree increments. The data reduction algorithm converted the instantaneous pressures to coefficient form, determined the wind speed and relative rotor position for the time step and then updated the number of readings, sum of the coefficients, and sum of the squares of the coefficients for each pressure transducer. For a particular run, the sum of the readings was divided by the number of readings to obtain the average value.

The standard deviation associated with a combination of wind speed and relative rotor position is an indication of the range of values of pressure coefficient. The mean values of the pressure coefficient for different runs repeat with variations much less than the corresponding standard deviations.

Because the surface pressures are a function of relative rotor position, the advantages gained by time averaging (5,6) could not

be utilized. This restriction also introduces some spreading of the data with respect to both wind speed and rotor position (5). A two-dimensional approach with no time averaging has been used successfully in the past to measure aerodynamic torques (7).

The mean and standard deviation for each transducer location were examined for each run. The mean values for different runs at the same wind speeds were compared to find further evidence of zero shifts. The magnitude of the standard deviations in the combined results in some instances also indicated problems with the data. Typical results from a single record are shown in Figure 7a to 7d. Figures 7a and 7b are for the transducer at the nose of the blade at high and low tip-speed ratios respectively. Figures 7c and 7d are for the transducer at $x/c = 0.05$ on the inner surface for the same tip-speed ratios.

The mean and standard deviation for the combined result from all records at the low tip-speed ratio are shown in Figures 8a and 8b. The band indicating plus or minus 1 standard deviation is wider than for the individual records in Figure 7. The mean values repeat from run to run with much less spread than the standard deviation. Effects of unsteady wind speed and direction contribute to the spread in the standard deviation.

3.4 Fits to Data

Several transducers were inoperative when the blade was mounted on the turbine so the full set listed in Table 1 was not available for the test. As the test program progressed several additional transducers failed, producing additional gaps in the

distribution of the taps along the blade. The final pressure transducer locations used in the data reduction are listed in Table 2. Pressure measurements at the same location on both sides of the blade were required to compute forces. The values of pressure coefficient available for the combined records were fit with a cubic spline on each side of the blade. The spline was evaluated at increments of x/c of 0.05 from the nose to the 0.95 location and was used to interpolate only. Each case was visually compared with the raw data to insure no artificial variations were introduced by interpolation. A typical comparison between the measured values and the fit curve is shown in Figure 9. The symbols represent the raw data on the inner and outer surface and the lines are the fit data.

3.5 CT/CN Calculation

The normal and tangential force coefficients, CN and CT, were obtained by integrating the interpolated pressure distributions. All integrations were done with respect to a coordinate system aligned with the chord of the blade as shown in Figure 6.

CN was calculated by taking the difference of the smoothed pressure coefficient values on either side of the blade and multiplying by the appropriate area. The pressure at the leading edge of the blade does not have a component in the normal direction and does not affect the normal force. CT was calculated using the product of the pressure coefficient and the area associated with a particular location projected in the tangential direction. Skin friction was neglected with this

approach. Therefore, the measured values of C_T will be larger than the actual values. The values of C_N should not be significantly affected by ignoring skin friction.

3.6 Angle of Attack

Wind-tunnel data for lift and drag are generally reported as a function of angle of attack. A direct measurement of angle of attack would facilitate comparison of the present data with published lift and drag data. Initially it was planned to measure the local angle of attack with the flow-angularity probe, but reliable measurements were not obtained. Reference 8 outlines some of the problems associated with the angle of attack measurements. The most reasonable approach seemed to be to base a calculation for angle of attack on the relative rotor position and incident wind speed measured with the flow-angularity probe. Two methods were considered, the first based strictly on geometry with no interference effects and the second based on a fixed wake aerodynamic model (9) incorporating both geometry and interference effects. The angles of attack computed using the fixed wake model agreed within one degree with those calculated with the vortex model, VDART, (10) and were the most convenient to use in the data reduction. All values of angle of attack used in the interpretation of the data were computed using the fixed wake model based on the measured relative rotor position and measured incident wind speed obtained using the flow-angularity probe.

4. RESULTS

4.1 Pressure coefficients

References 11 and 12 report pressure measurements for the NACA 0015 airfoil in terms of a pressure coefficient as a function of chord position, x/c , for a given angle of attack. This format is the logical starting point for examining the results of this experiment. It is important to remember that all results from this experiment have been averaged for many realizations of the same combination of incident wind speed and relative rotor position. This was a key choice in the data reduction as discussed in Section 3. Unsteady phenomena will not be evident in this format.

Pressure distributions for nominal angles of attack of 6, 8, and 12 degrees are shown in Figures 10 through 12, respectively. Each plot contains results for one side of the airfoil, either outer or inner. All angles of attack are positive, corresponding to the upwind half of the rotation. Data from two different tip-speed ratios were selected and compared with the predicted values obtained using the Eppler code (13). Results for the outer (pressure) surface are shown in Figure 10a for a nominal angle of attack of 6 degrees. A major difference between the measurements and predictions based on the Eppler code is evident from x/c of 0.1 to 0.3. The two sets of measurements at different tip-speed ratios are very similar. The stagnation point, indicated by the maximum positive pressure coefficient, is further back on the airfoil for the measurements than for the

predicted values. Aft of the stagnation point, the measured values indicate an acceleration of the flow (decrease in the pressure coefficient) and then a recovery or deceleration of the flow at an x/c of approximately 0.3. The symbols shown in these plots are for identification of the curves and are the interpolated values, not the actual data values. For the outer surface, transducers were located at x/c of 0.025, 0.05, 0.10, 0.15, 0.20, 0.25, and 0.30 as well as several locations on the rear of the airfoil. These measurement points are adequate to define the pressure distribution. The pressure distributions for the inner (suction) surface are shown in Figure 10b for the same angle of attack. The differences on this surface are not as great as those on the outer surface, but the agreement is still not exact. The measured pressure coefficient at the nose of the airfoil, $x/c = 0.0$, is less negative than the predictions, in some instances by a factor of 2. While the two different sets of measurements agree well in both plots, the value of the pressure on the leading edge is different in both cases.

Figures 11 and 12 show similar data for angles of attack of 8 and 12 degrees. The 12 degree case represents conditions approaching static stall for this airfoil at the operating Reynolds number. In all cases the comparisons are similar:

1. A local maximum in the distribution for the outer (pressure) surface between x/c of 0.1 and 0.3;
2. Pressures on the leading edge less negative than predicted;
3. Generally reasonable agreement on the inner (suction)

surface.

All calculations of force coefficients are based on these distributions. The normal force coefficients are the areas under these distributions. Even though the measured and predicted distributions differ, these differences tend to cancel upon integration. There are several possible explanations for the differences between the measured and predicted pressure distributions. First, the differences could be caused by curvilinear effects in the flow which could cause the shift of the stagnation point away from the leading edge on the outer (pressure) side of the airfoil.

Second, the transducers were covered with a thin Mylar film which was wrapped around the airfoil. While this film was mounted flush to the surface and very tight, there is a possibility that the film deformed during turbine operation. A slight bulge in the outer surface due to centrifugal forces could cause a variation in pressure on the outer surface observed in Figures 10-12.

A third possible explanation is a systematic error in either the pressure transducers or the data reduction process. Any possible systematic errors caused by wiring errors, transducer malfunctions, or zero offsets were carefully considered and ruled out.

The sequence of the data collection and the data reduction did not allow repeating the measurements for confirmation. No similar measurements on an operating vertical-axis wind turbine

are available for comparison. Many aspects of the measurements are very consistent, seem to be repeatable, and have very definite trends. However, the pressure distributions differ from two-dimensional airfoil data used in almost all aerodynamic and structural models. The remainder of the results and the conclusions should be considered in a qualitative as well as quantitative manner.

A second way to consider the pressure coefficients is in a format of pressure coefficient at a particular location as a function of relative rotor position as presented in Figures 13-16. This format has some similarity to an actual time history, but the coefficients shown have all been averaged for corresponding values of incident wind speed and relative rotor position. Results are included for four tip-speed ratios (TSR); 2.33, 3.09, 4.60, and 8.92. These were selected to illustrate the following conditions:

- | | |
|------------|---|
| TSR = 2.33 | stalled conditions |
| TSR = 3.09 | high power output, very little stall |
| TSR = 4.60 | low power output, no stall, near peak C_p |
| TSR = 8.92 | no power production, rotor motoring. |

Pressure coefficients at eight locations on the first third of the airfoil are shown in Figures 13a and 13b for a tip-speed ratio of 2.33. Data for the inner and outer surfaces are again shown separately. The results for the leading edge are shown on both plots as a point of reference. The stagnation point is near the leading edge, $x/c = 0.0$, for a relative rotor position

of 0 degrees corresponding to the blade moving upwind. The stagnation point is considered to be the location with the largest positive pressure coefficient. The stagnation point moves back on the outer surface of the blade with increasing relative rotor position, and shifts to the inner surface for the downwind half of the rotation (relative rotor positions from 180 to 360 degrees). A clear loss of negative pressure is evident on the outer surface and leading edge at a relative rotor position of 220 degrees. This loss also is evident in the force coefficients (Figures 22 and 30). The loss of negative pressure may be caused by an interaction with the wake of prior blade passages. Both the computed angle of attack and measured C_N values indicate that the loss of negative pressure does not correspond to stall of the airfoil. The reduction in negative pressure on the inner surface for relative rotor positions from 70 to 90 degrees is evidence of stall and originates from the trailing edge of the airfoil. There is a definite recovery in the negative pressure near the leading edge for relative rotor positions between 120 and 170 degrees.

Similar results are shown in Figures 14a and 14b for a tip-speed-ratio of 3.09. The negative pressures on the inner surface from relative rotor positions of 70 to 100 degrees indicate a decrease and subsequent recovery, perhaps an indication of the initiation of stall. The results at this tip-speed ratio show no evidence of wake interactions on the downwind portion of the rotation. Substantial upwind/downwind differences are evident in

the magnitude of the pressures. All pressure coefficients are based on the incident velocity measured on the blade. Therefore, the reduced negative pressure on the leading edge for the downwind portion of the rotation is caused by the reduced angle of attack, not reduced incident wind speed.

Results at tip-speed ratios of 4.60 and 8.92 are shown in Figures 15 and 16. For a tip-speed ratio of 8.92, the stagnation point remains on the outer surface of the blade for the entire rotation and is well aft of the leading edge.

These two formats for examining the surface pressures are combined into a three-dimensional format in Figures 17 to 20 for the same set of tip-speed ratios. These figures show the pressure coefficients as a function of both relative rotor position and chord location. Two view angles are shown for each case, and results are included for the outer surface, the inner surface, and the net or difference between these two surfaces. The integral of the net pressure coefficient as a function of x/c provides the normal force coefficient. These figures are useful for a qualitative interpretation of the data. The effects of stall in the region between 80 and 120 degrees relative rotor position and of the wake interaction near 220 degrees can be seen in the results for tip-speed ratio 2.33 as regions of decreased negative pressure. The local maximum in the pressure distributions (discussed in conjunction with Figures 10 and 11) as a function of x/c is clearly evident in all of the figures and is a consistent feature of the results.

4.2 Force Coefficients

All of the aerodynamic and structural models used to predict the performance or response of a wind turbine use airfoil section lift and drag data to calculate the forces acting on the blades. In most instances, these data come from wind-tunnel tests of two-dimensional sections. In order to compare the results of this experiment with two-dimensional section data, the averaged pressures were integrated to obtain normal and tangential force coefficients as defined by equations 2 and 3 and using the sign convention defined in Figure 6. In Figures 21-36, the measured values of force coefficient are compared with predicted values using (1) static airfoil data converted into tangential and normal format using the angle of attack based on the fixed-wake analysis and (2) a dynamic stall model based on the Gormont\Templin\Masse model (14,15). Each figure also includes the angle of attack calculated using the fixed wake analysis. Comparisons are made for more tip-speed ratios than were shown in the pressure distributions.

Several aspects of these data should be kept in mind when considering the following plots. The force coefficients are based on a local incident velocity which is a function of relative rotor position. It appears in all cases that the wake interaction on the downwind portion of the rotation prevents the onset of dynamic stall or similar phenomena. Therefore, the dynamic stall model was applied only on the upwind half of the rotation. The measured data are in 6 degree increments, but

symbols were only shown every 30 degrees to improve the clarity of the figures. The variations of the curves between symbols are based on actual data values.

Figures 21 to 28 present the comparison of the measured versus the predicted CN values for tip-speed ratios from 2.20 to 4.60. Figure 21 shows data at a tip-speed ratio of 2.20, well into stall for part of the rotation. For relative rotor positions from 0 to 90 degrees, the measured values and the predicted values using the dynamic stall model agree reasonably well. The measured CN increases up to a relative rotor position of 90 degrees and a corresponding calculated angle of attack of over 20 degrees. The agreement for the remainder of the rotation is not as good. The wake crossing in the range of relative rotor positions from 220 to 240 degrees is not predicted by either model. It is perhaps fortunate that even though the pressure distributions in this experiment differ significantly from the wind-tunnel measurements or analytical predictions, the integrated forces agree reasonably well.

Three key features of the CN values for a tip-speed ratio of 2.20 are: (1) the measured value of CN increases past the static stall value (1.09) and for angles of attack well beyond the static stall (this airfoil begins to stall at an angle of attack of 7 degrees for this Reynolds number); (2) the wake interaction on the downwind portion of the rotation substantially reduces the values of CN for negative angles of attack; (3) the post stall behavior in the range of relative rotor positions from 100 to 160

degrees differs substantially from the predictions. The increase in CN beyond static values is an indication that dynamic stall or a similar phenomena occurs. The maximum value of CN is less than that measured in wind-tunnel tests of dynamic stall. Nevertheless, for this situation CN increases beyond the static stall value and it increases for angles of attack well beyond static stall.

The results for tip-speed ratio of 2.33 are shown in Figure 22. These are similar to those for 2.20 except the downwind interaction is not as pronounced. At a tip speed ratio of 2.49, Figure 23, the downwind interaction is almost completely gone and the agreement between the measured and predicted values is better than for lower tip-speed ratios. At a tip-speed ratio of 2.66, Figure 24, the measured values of CN for the upwind portion of the rotation begin to consistently fall below the predictions by 5 to 10%. This decrease could be caused by the density of pressure taps near the leading edge of the airfoil. The spacing used may not have been sufficient to locate the peak negative pressure near the leading edge and hence may produce a normal force coefficient slightly less than the actual value. The results for a tip-speed ratio of 2.86 in Figure 25 are consistent with the previous data.

The wake interaction is no longer evident at a tip-speed ratio of 3.09, Figure 26. Some evidence of delay of stall is still evident on the upwind portion of the rotation. The post stall measurements in the range of relative rotor positions from 100 to

150 degrees are different from either set of predictions. At tip-speed ratios of 3.70 and 4.60, Figures 27 and 28, the measured results agree well with the predictions based on static stall for the entire rotation. Even though the CN agreement seems very good, keep in mind that the pressure distributions measured on the operating turbine are substantially different from wind-tunnel results or analytical predictions.

Tangential force coefficients were also calculated from the measured pressure distributions. The component of the pressure force parallel to the chord was integrated over the entire airfoil to obtain a tangential force coefficient. This coefficient was defined to be positive for a force in the direction of rotation. This sign convention is opposite to that used for drag force. The key pressure measurement location for the tangential force is on the leading edge; an error in this measurement will cause large errors in the calculated tangential force. This measurement location was not used in the calculation of the normal force coefficient. One of the major features of the measured pressure distributions was that the pressure on the leading edge was generally less negative in the measurements than the predictions. In addition, at a relative rotor position of 180 degrees (the blade is moving directly downwind), the pressure on the leading edge remains negative, causing a positive contribution to the tangential force coefficient.

The comparison of measured and predicted CT values are shown in Figures 29 to 36 for the same tip-speed ratios used for the CN

values. As with the CN comparisons, dynamic stall is only included on the upwind portion of the rotation. The results for a tip-speed ratio of 2.20 are shown in Figure 29. The measured and predicted values agree well up to a relative rotor position of 60 degrees. Beyond that point, the measured values of C_T are substantially greater than predicted and the measured value of C_T never returns to or even approaches zero when the blade is traveling directly downwind at a relative rotor position of 180 degrees. The measured peak value of C_T at this tip-speed ratio is between the value predicted by static stall and that predicted by dynamic stall. Larger measured than predicted C_T values in the range of relative rotor positions from 100 to 160 degrees were also observed in the accelerometer measurements of the same case (7). The wake interactions observed in the CN data at this tip-speed ratio seem to have very little effect on the C_T values.

The results for tip-speed ratios 2.33 and 2.49, Figures 30 and 31, are similar to those for a tip-speed ratio of 2.20. As the tip-speed ratio increases, the predictions on the upwind half of the rotation begin to change as the blade is no longer predicted to be in stall. The results for a tip-speed ratio of 2.66, Figure 32, exhibit reasonable agreement for the downwind portion of the rotation. The sharp drop in the predicted C_T values is not evident in the range of relative rotor position from 100 to 160 degrees and again the measured values of C_T do not approach zero at a relative rotor position of 180 degrees.

Results for a tip-speed ratio of 2.86 in Figure 33 show

improved agreement in the range of relative rotor positions from 100 to 160 degrees and good agreement on the downwind portion of the rotation. The CT values still do not approach zero at a relative rotor position of 180 degrees. The data in Figure 34 for a tip-speed ratio of 3.09 are similar to those for 2.86.

The data for tip-speed ratios of 3.70 and 4.60 in Figures 35 and 36 begin to show measured values of CT greater than predicted for the entire revolution. The shape of the curves agrees in a qualitative sense, but the measured values of CT again do not approach zero at a relative rotor position of 180 degrees. This increase in CT appears to be caused by the negative pressure on the leading edge of the airfoil; a pressure which is larger in magnitude than reported for wind-tunnel measurements. This effect was more evident as the tip-speed ratio increased beyond 4.60.

The data values shown in Figures 21 to 36 are tabulated in Tables 3 to 10.

5. CONCLUSIONS

The interpretation of these measurements is affected by some of the decisions in the data reduction and the method of data acquisition. This was a very complicated and difficult experiment, and the only data available for comparison were wind-tunnel results for two-dimensional models or overall torque or power coefficients for an entire turbine. The measurements presented in this report are for a single location on a single turbine blade. The experiment was conducted on an operating wind turbine in a turbulent field environment. Hopefully, future work will provide confirmation of some of the key observations.

Analysis of the pressure data from this test leads to the following conclusions:

1. There is a definite increase in the normal force coefficients beyond those predicted by static airfoil data. This is an indication of either dynamic stall or a phenomena similar to dynamic stall. This increase was evident for tip-speed ratios from 2.20 to 3.09.

2. The measured pressure distributions differ from two-dimensional section data. Substantial differences are evident between the pressure distributions on the inner and outer surfaces.

3. At low tip-speed ratios downwind interference effects were observed. These effects momentarily reduce the normal force coefficient and may be caused by wake crossings. These effects were not observed for tip-speed ratios greater than 3.09.

4. Very clear upwind/downwind differences were found. All results were presented in terms of a pressure or force coefficient based on the incident velocity measured with the total velocity probe, so the reduction in the velocity for the downwind portion of the rotation was included in the coefficients.

5. There was no evidence of any increase in normal force coefficient beyond that predicted by two-dimensional static section data for the downwind portion of the rotation of the turbine.

Future experimental measurements should incorporate instrumentation to measure both the incident speed and angle of attack. Unsteady flow visualization should be used to aid in the interpretation of the pressure measurements. The density of the taps near the leading edge of the airfoil should be much greater than was used in this study. The shape of the airfoil section at the test location should be carefully verified with the blade mounted on the turbine. The most important thrust of any future work examining the pressure distribution on an operating vertical axis wind turbine should be to verify the anomalous pressure distributions observed in this study.

REFERENCES

1. F. Johnston, Jr., ed, Proceedings of the Vertical-Axis Wind Turbine (VAWT) Design Technology Seminar for Industry, SAND80-0984 (Albuquerque, NM: Sandia National Laboratories, 1980).
2. R.E. Akins, "Wind Characteristics for Field Testing of Wind Energy Conversion Systems," SAND78-1563 (Albuquerque, NM: Sandia National Laboratories, 1978).
3. R.E. Akins, "Wind Characteristics at the VAWT Test Facility," SAND78-0760 (Albuquerque, NM: Sandia National Laboratories, 1978).
4. R.E. Akins, "Performance Evaluation of Wind Energy Conversion Systems Using the Method of Bins - Current Status," SAND77-1375 (Albuquerque, NM: Sandia National Laboratories, 1978).
5. R.E. Akins, "Method-of-Bins Update," Proceedings of Wind Energy Expo '82 (Amarillo, TX: American Wind Energy Association, October 1982).
6. T.E. Hausfeld and C.A. Hansen, "A Systematic Approach to Using the Method of Bins," Proceedings of the Sixth Biennial Wind Energy Conference (Minneapolis, MN: American Solar Energy Society, June 1983).
7. R.E. Akins, D.E. Berg, and W.T. Cyrus, "Measurements and Calculations of Aerodynamic Torques for a Vertical-Axis Wind Turbine," SAND86-2164 (Albuquerque, NM: Sandia National Laboratories, 1987).
8. R.E. Akins, P.C. Klimas, and R.H. Croll, "Pressure Distributions on an Operating Vertical Axis Wind Turbine Blade Element," Proceedings of the Sixth Biennial Wind Energy Conference (Minneapolis, MN: American Solar Energy Society, June 1983).
9. R.E. Wilson and S.N. Walker, "Fixed Wake Analysis of the Darrieus Rotor," SAND81-7026 (Albuquerque, NM: Sandia National Laboratories, 1981).
10. J.H. Strickland, B.T. Webster, and T. Nguyen, "A Vortex Model of the Darrieus Turbine: An Analytical and Experimental Study," SAND79-7058 (Albuquerque, NM: Sandia National Laboratories, 1980).
11. A. Pope, "The Forces and Moments Over an NACA 0015 Airfoil Through 180 Degrees Angle of Attack," Aero Digest (Vol. 58, No.4, April 1949).

12. S.J. Miley, "A Catalog of Low Reynolds Number Airfoil Data for Wind Turbine Applications," RFP-3387 (Golden, CO: Rockwell International Corporation, February 1982).
13. R. Eppler, and D. Somers, "A Computer Program for the Design and Analysis of Low-Speed Airfoils," NASA TM-80210, (Langley, VA: NASA, 1980).
14. R.E. Gormont, "A Mathematical Model of Unsteady Aerodynamics and Radial Flow for Application to Helicopter Rotors," USAAMRDL Technical Report 72-67 (Philadelphia, PA: Boeing Company, 1973).
15. B. Masse, "Description de deux programmes d'ordinateur pour le calcul de performances et des charges aerodynamiques pour les eoliennes a axe vertical," IREQ-2379 (Varenes, Canada: Institut de Recherche d'Hydro-Quebec, 1981).

TABLE 1. Pressure transducer locations on the inner and outer surface of blade (as a fraction of chord).

X/C
 0.000
 0.025
 0.050
 0.100
 0.150
 0.200
 0.250
 0.350
 0.400
 0.500
 0.600
 0.700
 0.800
 0.950

TABLE 2. Transducer locations used in the data analysis.
 (All locations in x/c)

<u>INNER SURFACE</u>	<u>OUTER SURFACE</u>
0.000	0.000
0.050	0.025
0.100	0.050
0.150	0.100
0.250	0.150
0.300	0.200
0.500	0.250
0.700	0.300
0.950	0.500
	0.700
	0.950

TABLE 3. CN and CT for Tip-speed ratio 2.20.

RRP	AOA	CN	CT	RRP	AOA	CN	CT
3.	0.9	0.047	0.027	183.	-2.4	-0.196	0.158
9.	2.8	0.225	0.037	189.	-6.9	-0.467	0.186
15.	4.6	0.370	0.049	195.	-10.6	-0.739	0.257
21.	6.4	0.459	0.076	201.	-13.6	-0.740	0.254
27.	8.1	0.629	0.126	207.	-16.0	-0.693	0.220
33.	9.8	0.755	0.168	213.	-17.8	-0.766	0.276
39.	11.5	0.846	0.204	219.	-19.0	-0.006	0.122
45.	13.1	0.950	0.230	225.	-19.9	1.080	0.117
51.	14.6	1.040	0.252	231.	-20.4	0.268	0.098
57.	16.0	1.115	0.271	237.	-20.6	0.526	0.079
63.	17.4	1.146	0.276	243.	-20.7	-0.327	0.115
69.	18.7	1.195	0.271	249.	-20.5	-0.336	0.067
75.	20.0	1.184	0.243	255.	-20.2	-0.702	0.091
81.	21.1	1.066	0.204	261.	-19.8	-1.060	0.135
87.	22.1	1.120	0.238	267.	-19.2	-0.896	0.101
93.	23.0	1.144	0.211	273.	-18.6	-1.004	0.136
99.	23.7	1.010	0.199	279.	-17.9	-1.014	0.148
105.	24.3	0.964	0.153	285.	-17.1	-1.127	0.177
111.	24.6	0.920	0.144	291.	-16.2	-1.095	0.164
117.	24.8	0.949	0.161	297.	-15.2	-1.056	0.172
123.	24.7	0.959	0.153	303.	-14.2	-1.051	0.168
129.	24.2	0.992	0.153	309.	-13.1	-0.957	0.158
135.	23.4	0.983	0.171	315.	-11.9	-0.924	0.143
141.	22.1	0.770	0.155	321.	-10.6	-0.869	0.129
147.	20.4	0.658	0.137	327.	-9.2	-0.815	0.112
153.	18.0	0.575	0.125	333.	-7.7	-0.730	0.093
159.	15.0	0.434	0.124	339.	-6.1	-0.615	0.071
165.	11.4	0.329	0.127	345.	-4.5	-0.516	0.052
171.	7.2	0.111	0.134	351.	-2.7	-0.196	0.017
177.	2.5	0.134	0.140	357.	-0.9	-0.082	0.018

TABLE 4. CN and CT for Tip-speed ratio 2.33.

RRP	AOA	CN	CT	RRP	AOA	CN	CT
3.	0.9	-0.031	0.012	183.	-2.2	-0.119	0.151
9.	2.7	0.137	0.016	189.	-6.2	-0.380	0.167
15.	4.4	0.304	0.037	195.	-9.6	-0.467	0.199
21.	6.1	0.430	0.060	201.	-12.4	-0.681	0.244
27.	7.8	0.630	0.113	207.	-14.6	-0.653	0.241
33.	9.4	0.765	0.156	213.	-16.2	-0.268	0.191
39.	11.0	0.812	0.183	219.	-17.4	-0.580	0.218
45.	12.5	0.929	0.212	225.	-18.2	-0.458	0.164
51.	13.9	0.972	0.217	231.	-18.7	-0.562	0.141
57.	15.3	1.096	0.251	237.	-19.0	-0.708	0.134
63.	16.6	1.146	0.255	243.	-19.0	-0.776	0.133
69.	17.8	1.226	0.268	249.	-18.9	-0.932	0.141
75.	18.9	1.218	0.256	255.	-18.7	-1.008	0.148
81.	19.9	1.201	0.259	261.	-18.3	-0.977	0.131
87.	20.9	1.208	0.222	267.	-17.9	-1.064	0.141
93.	21.7	1.075	0.187	273.	-17.3	-1.052	0.162
99.	22.3	1.094	0.184	279.	-16.7	-1.075	0.193
105.	22.8	1.016	0.156	285.	-16.0	-1.141	0.189
111.	23.1	1.012	0.157	291.	-15.2	-1.009	0.151
117.	23.2	1.065	0.166	297.	-14.3	-0.996	0.149
123.	23.0	1.162	0.183	303.	-13.4	-0.905	0.122
129.	22.5	1.158	0.175	309.	-12.3	-0.870	0.118
135.	21.6	1.074	0.166	315.	-11.2	-0.837	0.135
141.	20.4	0.919	0.150	321.	-10.0	-0.773	0.116
147.	18.7	0.859	0.154	327.	-8.7	-0.684	0.089
153.	16.5	0.733	0.146	333.	-7.3	-0.589	0.066
159.	13.7	0.550	0.142	339.	-5.8	-0.506	0.058
165.	10.3	0.468	0.146	345.	-4.3	-0.351	0.031
171.	6.5	0.335	0.138	351.	-2.6	-0.296	0.024
177.	2.2	0.106	0.144	357.	-0.9	-0.157	0.017

TABLE 5. CN and CT for Tip-speed ratio 2.49.

RRP	AOA	CN	CT	RRP	AOA	CN	CT
3.	0.9	-0.002	0.013	183.	-2.0	-0.004	0.144
9.	2.5	0.131	0.019	189.	-5.5	-0.199	0.159
15.	4.2	0.296	0.040	195.	-8.6	-0.428	0.203
21.	5.8	0.437	0.061	201.	-11.1	-0.564	0.213
27.	7.4	0.559	0.089	207.	-13.1	-0.757	0.259
33.	8.9	0.693	0.132	213.	-14.6	-0.853	0.274
39.	10.4	0.809	0.174	219.	-15.7	-0.838	0.262
45.	11.8	0.909	0.217	225.	-16.5	-0.639	0.229
51.	13.2	0.975	0.252	231.	-17.0	-0.869	0.228
57.	14.4	1.026	0.261	237.	-17.2	-0.879	0.177
63.	15.6	1.084	0.272	243.	-17.3	-0.889	0.147
69.	16.7	1.114	0.277	249.	-17.2	-1.020	0.142
75.	17.8	1.193	0.274	255.	-17.0	-1.036	0.138
81.	18.7	1.147	0.241	261.	-16.7	-1.032	0.143
87.	19.5	1.137	0.229	267.	-16.4	-1.017	0.157
93.	20.2	1.045	0.209	273.	-15.9	-1.010	0.158
99.	20.8	0.986	0.189	279.	-15.4	-1.089	0.175
105.	21.2	1.029	0.184	285.	-14.8	-1.057	0.161
111.	21.4	1.045	0.178	291.	-14.1	-1.027	0.153
117.	21.4	1.029	0.168	297.	-13.3	-1.001	0.151
123.	21.1	1.030	0.176	303.	-12.5	-0.934	0.142
129.	20.6	1.019	0.183	309.	-11.5	-0.877	0.130
135.	19.8	0.972	0.180	315.	-10.5	-0.849	0.122
141.	18.6	0.959	0.173	321.	-9.4	-0.824	0.116
147.	16.9	0.901	0.155	327.	-8.2	-0.739	0.094
153.	14.9	0.758	0.143	333.	-6.9	-0.657	0.074
159.	12.3	0.619	0.132	339.	-5.5	-0.543	0.051
165.	9.3	0.464	0.132	345.	-4.1	-0.451	0.037
171.	5.8	0.295	0.132	351.	-2.5	-0.280	0.022
177.	2.0	0.172	0.128	357.	-0.9	-0.193	0.014

TABLE 6. CN and CT for Tip-speed ratio 2.66.

RRP	AOA	CN	CT	RRP	AOA	CN	CT
3.	0.8	0.018	0.019	183.	-1.8	0.061	0.154
9.	2.4	0.170	0.029	189.	-5.0	-0.111	0.154
15.	4.0	0.344	0.049	195.	-7.7	-0.304	0.173
21.	5.5	0.476	0.078	201.	-10.0	-0.463	0.197
27.	7.0	0.591	0.110	207.	-11.8	-0.487	0.192
33.	8.5	0.680	0.140	213.	-13.1	-0.629	0.217
39.	9.9	0.767	0.174	219.	-14.2	-0.612	0.221
45.	11.2	0.871	0.209	225.	-14.9	-0.514	0.211
51.	12.4	0.907	0.231	231.	-15.4	-0.066	0.210
57.	13.6	0.973	0.258	237.	-15.6	-0.837	0.234
63.	14.7	1.036	0.272	243.	-15.7	-0.754	0.183
69.	15.7	1.055	0.271	249.	-15.6	-0.928	0.200
75.	16.7	1.091	0.272	255.	-15.5	-0.906	0.167
81.	17.5	1.091	0.263	261.	-15.3	-0.956	0.174
87.	18.2	1.052	0.244	267.	-15.0	-0.948	0.175
93.	18.8	1.043	0.230	273.	-14.6	-0.980	0.179
99.	19.3	1.044	0.215	279.	-14.1	-1.013	0.182
105.	19.6	1.032	0.202	285.	-13.6	-0.986	0.176
111.	19.8	1.015	0.188	291.	-13.0	-0.962	0.164
117.	19.7	1.026	0.194	297.	-12.3	-0.918	0.147
123.	19.5	1.060	0.199	303.	-11.6	-0.902	0.140
129.	18.9	1.054	0.201	309.	-10.8	-0.844	0.125
135.	18.1	1.026	0.195	315.	-9.8	-0.802	0.112
141.	16.9	1.029	0.201	321.	-8.8	-0.727	0.095
147.	15.4	0.924	0.195	327.	-7.7	-0.655	0.077
153.	13.5	0.808	0.175	333.	-6.5	-0.576	0.060
159.	11.1	0.698	0.169	339.	-5.2	-0.484	0.045
165.	8.3	0.554	0.162	345.	-3.9	-0.394	0.032
171.	5.2	0.412	0.150	351.	-2.4	-0.246	0.020
177.	1.8	0.222	0.153	357.	-0.8	-0.079	0.015

TABLE 7. CN and CT for Tip-speed ratio 2.86.

RRP	AOA	CN	CT	RRP	AOA	CN	CT
3.	0.8	0.034	0.017	183.	-1.6	0.116	0.157
9.	2.3	0.197	0.031	189.	-4.4	-0.162	0.168
15.	3.8	0.365	0.052	195.	-6.9	-0.321	0.176
21.	5.2	0.485	0.079	201.	-8.9	-0.473	0.188
27.	6.6	0.612	0.110	207.	-10.5	-0.592	0.207
33.	8.0	0.707	0.142	213.	-11.7	-0.663	0.212
39.	9.3	0.795	0.177	219.	-12.7	-0.772	0.234
45.	10.5	0.867	0.208	225.	-13.3	-0.818	0.224
51.	11.7	0.917	0.234	231.	-13.7	-0.860	0.233
57.	12.7	0.980	0.259	237.	-14.0	-0.941	0.239
63.	13.8	1.015	0.272	243.	-14.1	-0.987	0.230
69.	14.7	1.059	0.282	249.	-14.1	-0.861	0.193
75.	15.5	1.080	0.283	255.	-14.0	-0.620	0.126
81.	16.3	1.080	0.274	261.	-13.8	-0.993	0.203
87.	16.9	1.100	0.269	267.	-13.5	-1.009	0.197
93.	17.4	1.028	0.245	273.	-13.2	-1.002	0.193
99.	17.8	1.055	0.245	279.	-12.8	-1.023	0.193
105.	18.1	1.045	0.238	285.	-12.4	-1.003	0.184
111.	18.2	0.978	0.218	291.	-11.9	-1.002	0.176
117.	18.1	0.828	0.202	297.	-11.3	-0.989	0.166
123.	17.8	0.668	0.167	303.	-10.7	-0.921	0.150
129.	17.2	0.905	0.203	309.	-9.9	-0.873	0.132
135.	16.4	1.028	0.226	315.	-9.1	-0.821	0.116
141.	15.3	1.001	0.225	321.	-8.2	-0.737	0.096
147.	13.9	0.941	0.214	327.	-7.2	-0.660	0.079
153.	12.1	0.828	0.201	333.	-6.1	-0.564	0.060
159.	10.0	0.760	0.190	339.	-4.9	-0.479	0.046
165.	7.5	0.671	0.190	345.	-3.6	-0.360	0.032
171.	4.7	0.531	0.180	351.	-2.2	-0.226	0.022
177.	1.6	0.317	0.160	357.	-0.8	-0.093	0.018

TABLE 8. CN and CT for Tip-speed ratio 3.09.

RRP	AOA	CN	CT	RRP	AOA	CN	CT
3.	0.7	0.029	0.021	183.	-1.4	0.146	0.145
9.	2.2	0.199	0.032	189.	-3.9	-0.106	0.153
15.	3.6	0.352	0.053	195.	-6.1	-0.307	0.167
21.	4.9	0.492	0.081	201.	-7.9	-0.453	0.178
27.	6.2	0.608	0.110	207.	-9.3	-0.589	0.190
33.	7.5	0.714	0.148	213.	-10.4	-0.709	0.210
39.	8.7	0.787	0.172	219.	-11.2	-0.773	0.224
45.	9.8	0.855	0.201	225.	-11.8	-0.837	0.235
51.	10.9	0.909	0.223	231.	-12.2	-0.901	0.243
57.	11.9	0.956	0.246	237.	-12.4	-0.952	0.243
63.	12.8	1.003	0.268	243.	-12.5	-0.968	0.236
69.	13.6	1.037	0.281	249.	-12.5	-0.987	0.229
75.	14.3	1.061	0.288	255.	-12.4	-0.972	0.209
81.	15.0	1.091	0.290	261.	-12.3	-0.949	0.192
87.	15.5	1.095	0.283	267.	-12.0	-0.946	0.183
93.	16.0	1.079	0.271	273.	-11.8	-0.949	0.181
99.	16.3	1.090	0.264	279.	-11.5	-0.946	0.174
105.	16.5	1.084	0.254	285.	-11.1	-0.942	0.165
111.	16.5	1.086	0.253	291.	-10.7	-0.924	0.157
117.	16.4	1.089	0.252	297.	-10.3	-0.902	0.144
123.	16.1	1.099	0.257	303.	-9.7	-0.850	0.129
129.	15.6	1.079	0.253	309.	-9.1	-0.798	0.113
135.	14.8	1.037	0.244	315.	-8.4	-0.735	0.095
141.	13.8	1.019	0.246	321.	-7.6	-0.676	0.082
147.	12.4	0.946	0.222	327.	-6.7	-0.605	0.066
153.	10.8	0.887	0.209	333.	-5.7	-0.515	0.050
159.	8.9	0.806	0.201	339.	-4.6	-0.433	0.038
165.	6.7	0.658	0.174	345.	-3.4	-0.330	0.027
171.	4.1	0.527	0.165	351.	-2.1	-0.214	0.021
177.	1.4	0.326	0.153	357.	-0.7	-0.076	0.017

TABLE 9. CN and CT for Tip-speed ratio 3.70.

RRP	AOA	CN	CT	RRP	AOA	CN	CT
3.	0.6	-0.002	0.025	183.	-1.1	0.151	0.131
9.	1.9	0.141	0.036	189.	-3.0	-0.058	0.137
15.	3.1	0.270	0.050	195.	-4.7	-0.259	0.151
21.	4.2	0.368	0.073	201.	-6.0	-0.407	0.164
27.	5.3	0.522	0.104	207.	-7.1	-0.562	0.187
33.	6.4	0.617	0.132	213.	-7.9	-0.651	0.199
39.	7.4	0.714	0.164	219.	-8.5	-0.740	0.207
45.	8.3	0.774	0.190	225.	-8.9	-0.788	0.207
51.	9.2	0.833	0.213	231.	-9.1	-0.832	0.205
57.	9.9	0.879	0.237	237.	-9.3	-0.864	0.202
63.	10.7	0.928	0.257	243.	-9.3	-0.859	0.194
69.	11.3	0.969	0.271	249.	-9.3	-0.874	0.184
75.	11.8	1.004	0.285	255.	-9.3	-0.864	0.174
81.	12.3	1.037	0.295	261.	-9.2	-0.865	0.164
87.	12.7	1.028	0.300	267.	-9.0	-0.863	0.157
93.	13.0	1.062	0.298	273.	-8.9	-0.848	0.149
99.	13.2	1.037	0.295	279.	-8.7	-0.849	0.143
105.	13.3	1.048	0.288	285.	-8.5	-0.834	0.133
111.	13.3	1.054	0.282	291.	-8.3	-0.816	0.122
117.	13.1	1.027	0.275	297.	-8.0	-0.775	0.112
123.	12.8	1.014	0.270	303.	-7.7	-0.777	0.104
129.	12.3	0.993	0.262	309.	-7.3	-0.734	0.095
135.	11.7	0.967	0.246	315.	-6.8	-0.675	0.084
141.	10.8	0.913	0.234	321.	-6.2	-0.630	0.069
147.	9.7	0.873	0.219	327.	-5.5	-0.562	0.059
153.	8.4	0.792	0.193	333.	-4.8	-0.482	0.045
159.	6.9	0.712	0.173	339.	-3.9	-0.397	0.034
165.	5.1	0.638	0.157	345.	-2.9	-0.308	0.025
171.	3.2	0.508	0.143	351.	-1.8	-0.204	0.020
177.	1.1	0.321	0.133	357.	-0.6	-0.086	0.020

TABLE 10. CN and CT for Tip-speed ratio 4.60.

RRP	AOA	CN	CT	RRP	AOA	CN	CT
3.	0.5	-0.028	0.038	183.	-0.8	0.154	0.131
9.	1.6	0.071	0.045	189.	-2.2	0.030	0.134
15.	2.6	0.187	0.063	195.	-3.4	-0.139	0.138
21.	3.5	0.280	0.080	201.	-4.4	-0.255	0.146
27.	4.4	0.411	0.101	207.	-5.1	-0.370	0.152
33.	5.2	0.500	0.122	213.	-5.6	-0.473	0.159
39.	6.0	0.580	0.142	219.	-5.9	-0.524	0.157
45.	6.7	0.648	0.163	225.	-6.2	-0.588	0.160
51.	7.3	0.722	0.185	231.	-6.3	-0.614	0.155
57.	7.9	0.781	0.208	237.	-6.3	-0.662	0.157
63.	8.4	0.820	0.223	243.	-6.3	-0.670	0.148
69.	8.9	0.867	0.245	249.	-6.3	-0.671	0.142
75.	9.2	0.893	0.254	255.	-6.2	-0.716	0.139
81.	9.6	0.918	0.261	261.	-6.1	-0.718	0.131
87.	9.8	0.929	0.268	267.	-6.1	-0.683	0.122
93.	10.0	0.942	0.272	273.	-6.0	-0.692	0.118
99.	10.1	0.951	0.275	279.	-5.9	-0.691	0.109
105.	10.1	0.940	0.271	285.	-5.9	-0.685	0.104
111.	10.0	0.946	0.267	291.	-5.8	-0.670	0.101
117.	9.9	0.943	0.263	297.	-5.7	-0.668	0.092
123.	9.6	0.907	0.252	303.	-5.5	-0.628	0.084
129.	9.2	0.896	0.241	309.	-5.3	-0.610	0.076
135.	8.7	0.862	0.232	315.	-5.1	-0.578	0.068
141.	8.1	0.827	0.217	321.	-4.7	-0.526	0.061
147.	7.3	0.776	0.195	327.	-4.3	-0.488	0.054
153.	6.3	0.708	0.181	333.	-3.8	-0.424	0.045
159.	5.1	0.621	0.163	339.	-3.1	-0.363	0.041
165.	3.8	0.549	0.148	345.	-2.4	-0.289	0.036
171.	2.4	0.417	0.137	351.	-1.5	-0.215	0.033
177.	0.8	0.293	0.133	357.	-0.5	-0.106	0.034

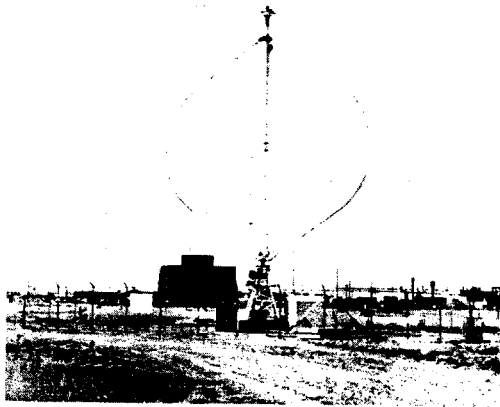


Figure 1. Sandia/DOE Research Turbine, Albuquerque, NM.

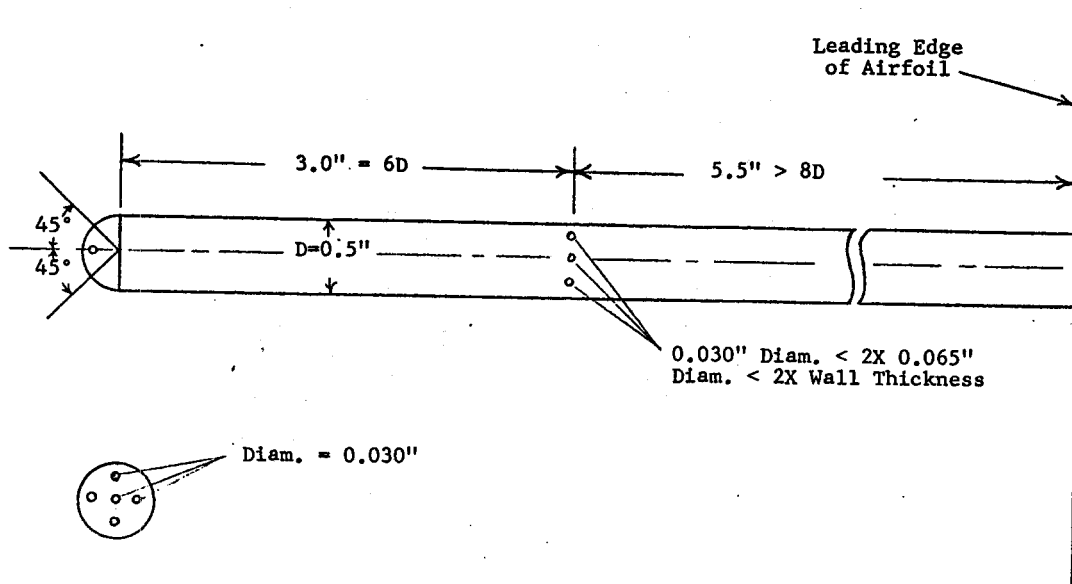


Figure 2. Flow-Angularity Probe used in the Test Program.

MOUNTING OF SURFACE PRESSURE TRANSDUCERS

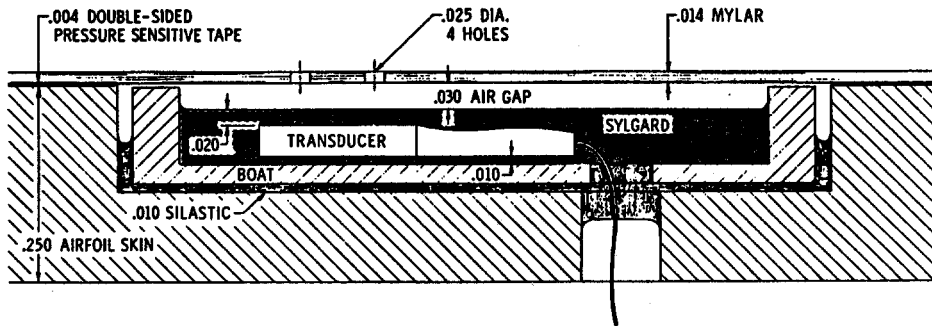


Figure 3. Pressure Transducer Mounting Arrangement.

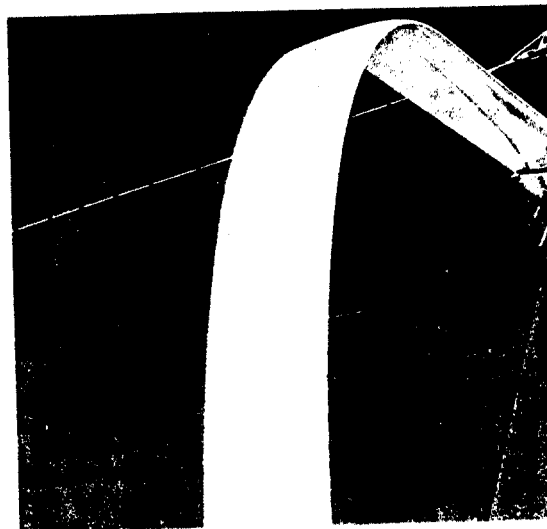


Figure 4. Pressure Transducers Installed on Turbine.

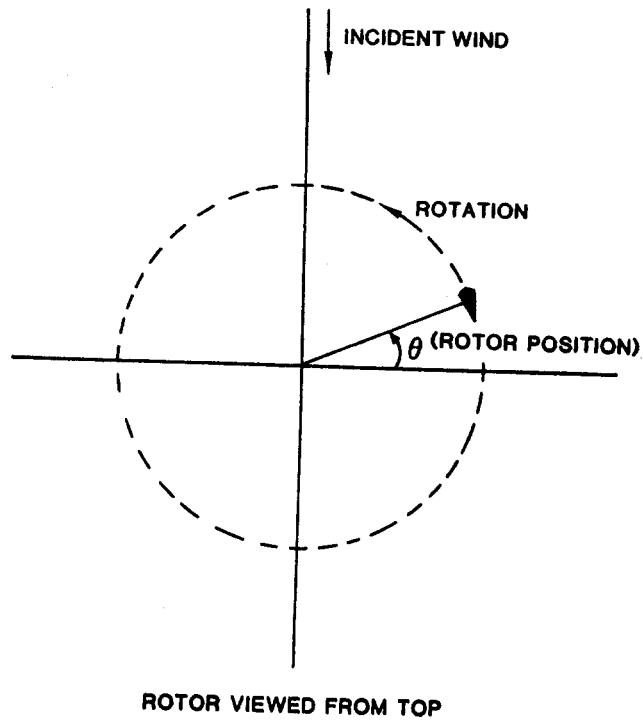


Figure 5. Nomenclature used in Defining Relative Rotor Position.

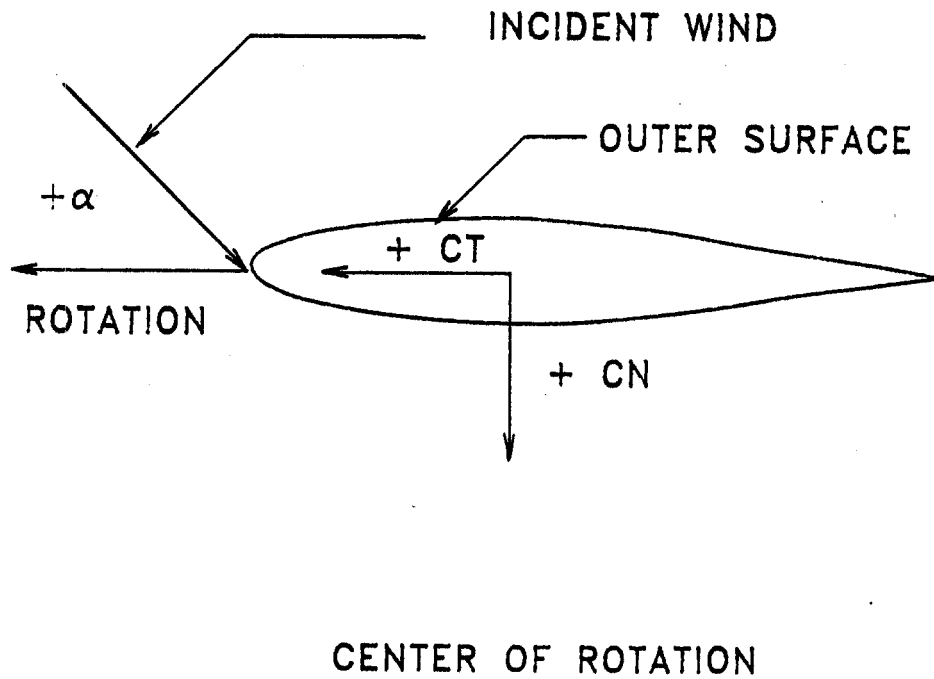


Figure 6. Sign Convention used with Force Coefficients.

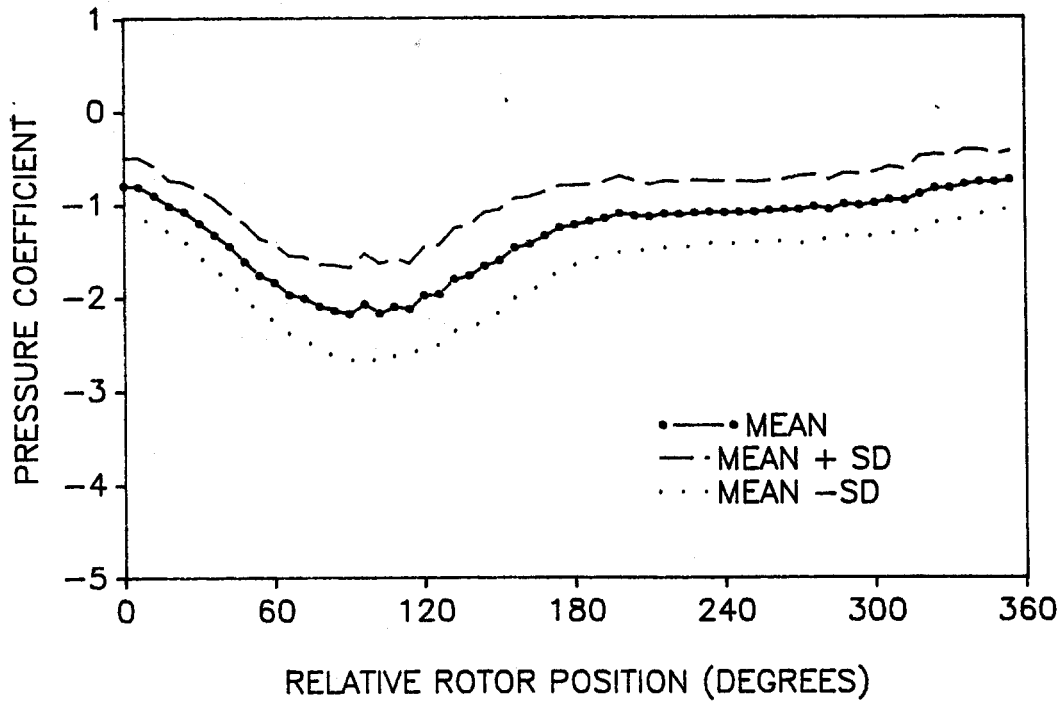


Figure 7a. Variation in Pressure Coefficients Single Record:
 $x/c = 0.00$, Tip-speed ratio 7.98.

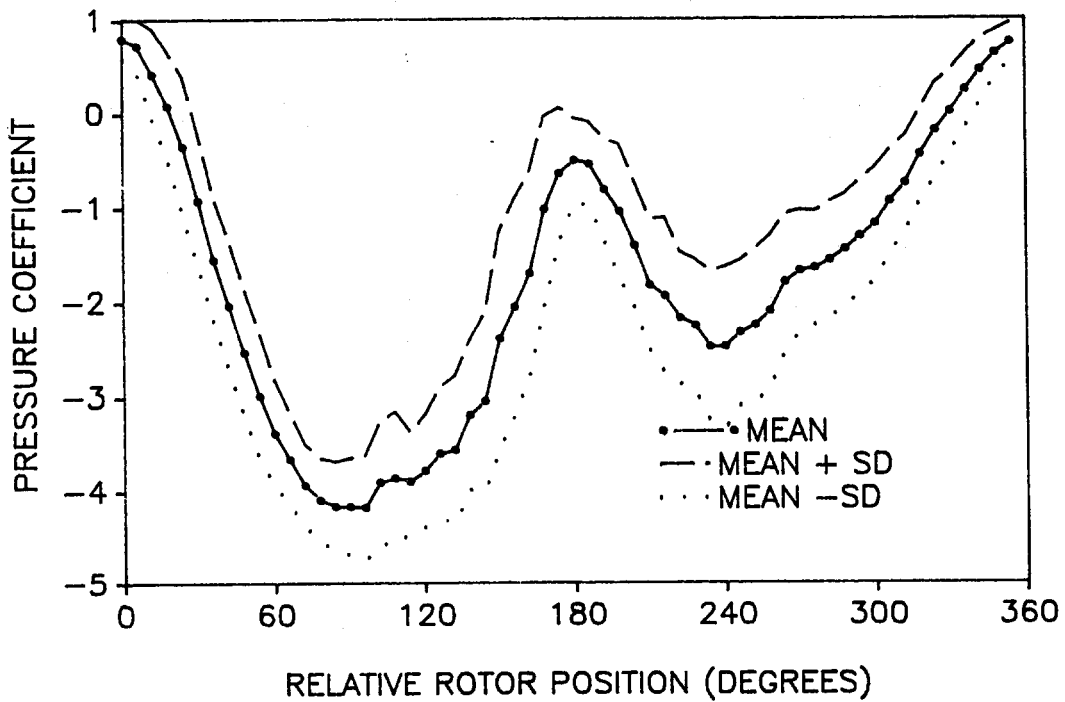


Figure 7b. Variation in Pressure Coefficients Single Record:
 $x/c = 0.00$, Tip-speed ratio 3.23.

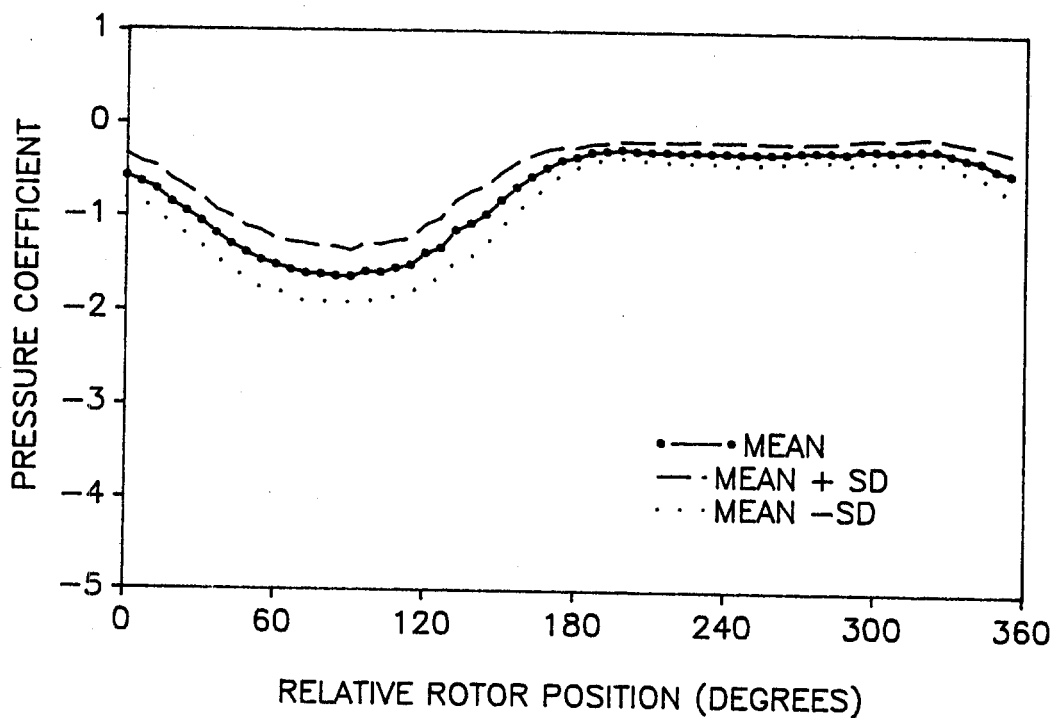


Figure 7c. Variation in Pressure Coefficients Single Record:
 $x/c = 0.05$, Tip-speed ratio 7.98.

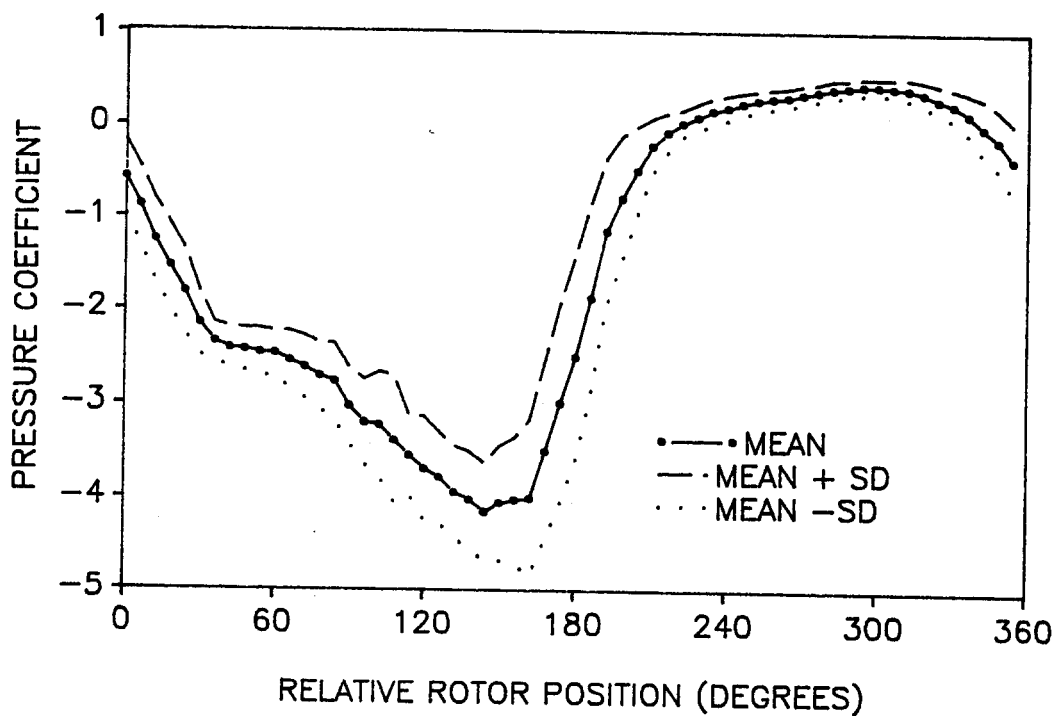


Figure 7d. Variation in Pressure Coefficients Single Record:
 $x/c = 0.05$, Tip-speed ratio 3.23.

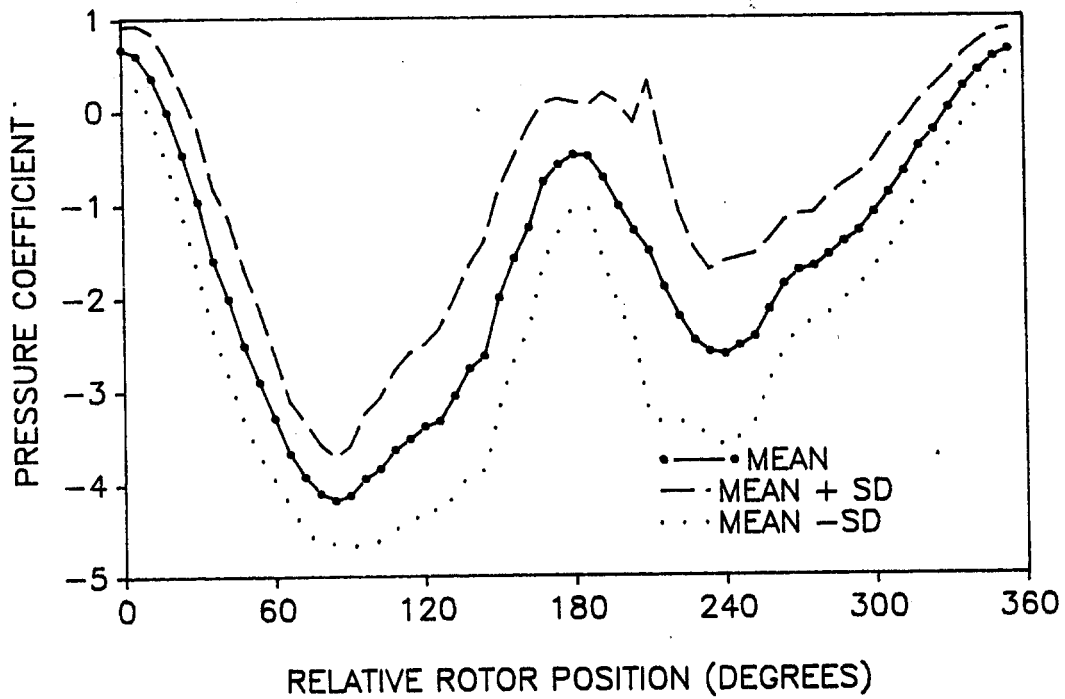


Figure 8a. Variation in Pressure Coefficients Combined Record:
 $x/c = 0.00$, Tip-speed ratio 3.09.

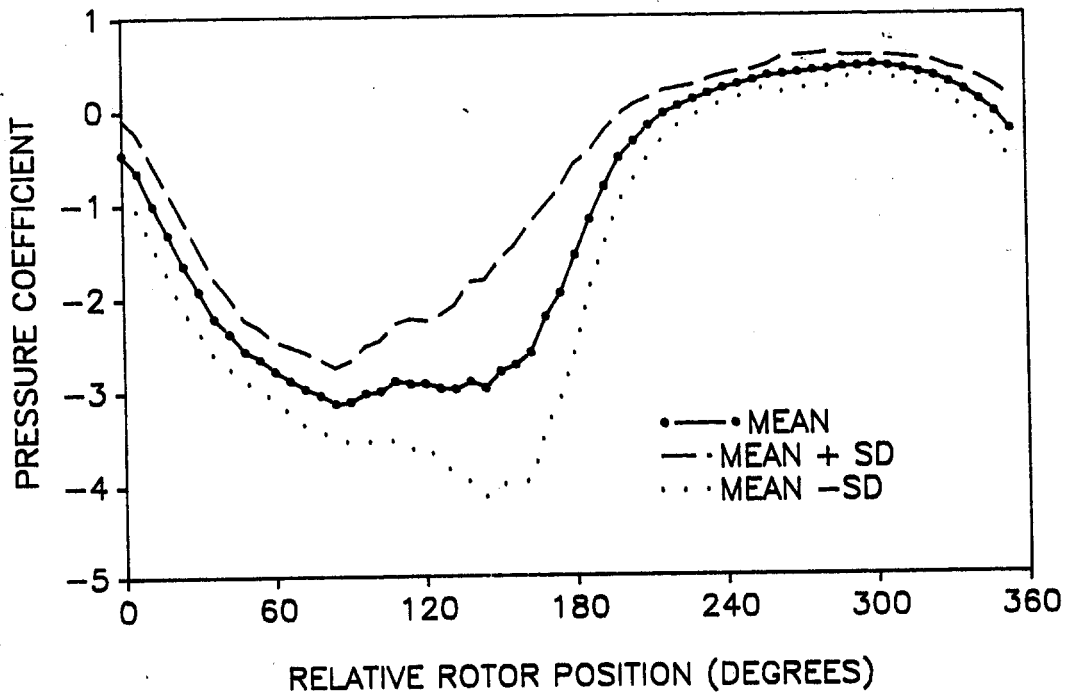


Figure 8b. Variation in Pressure Coefficients Combined Record:
 $x/c = 0.05$, Tip-speed ratio 3.09.

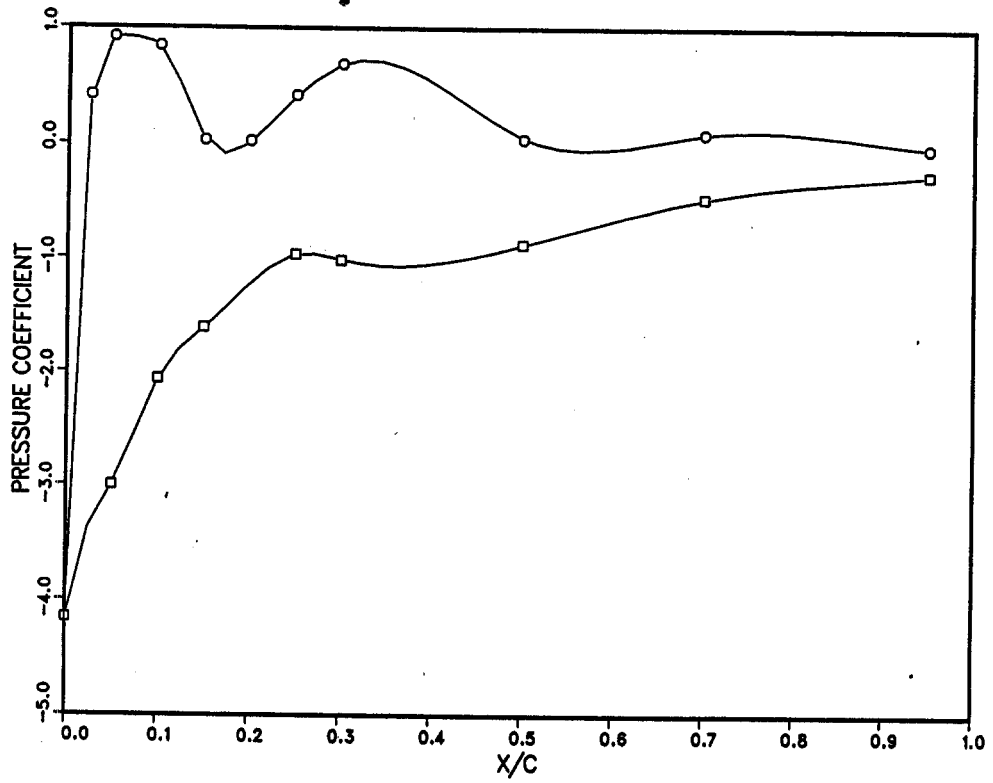


Figure 9. Example of Curve Fit, Pressure Distributions.

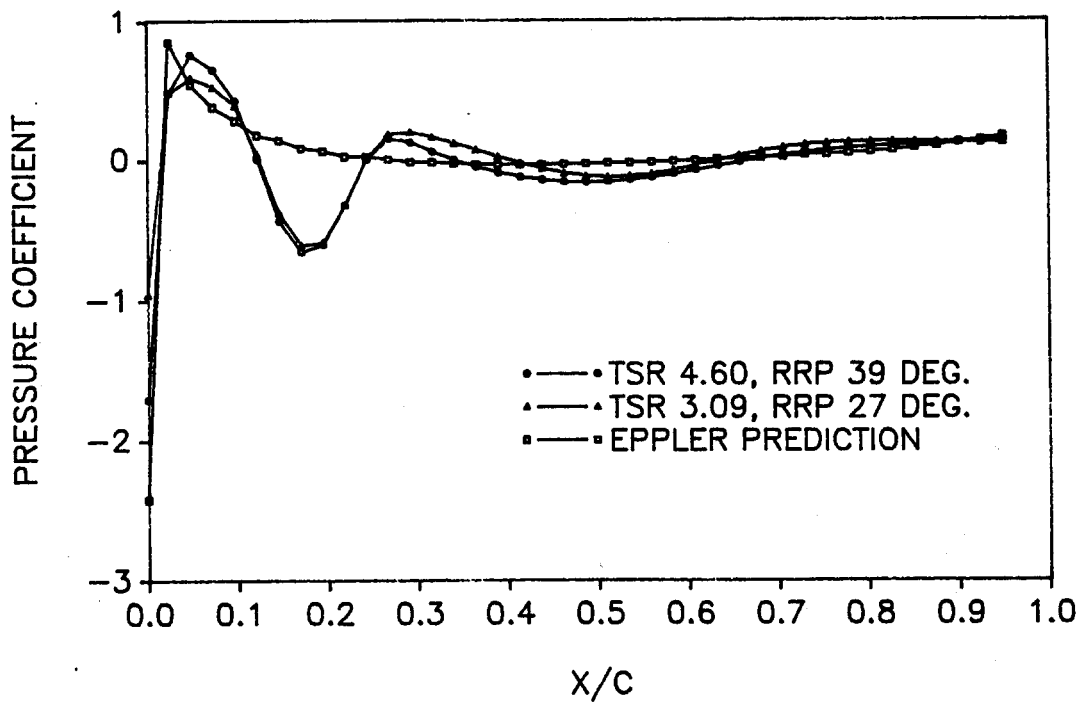


Figure 10a. Pressure Distribution Outer Surface:
Angle of Attack 6 Degrees.

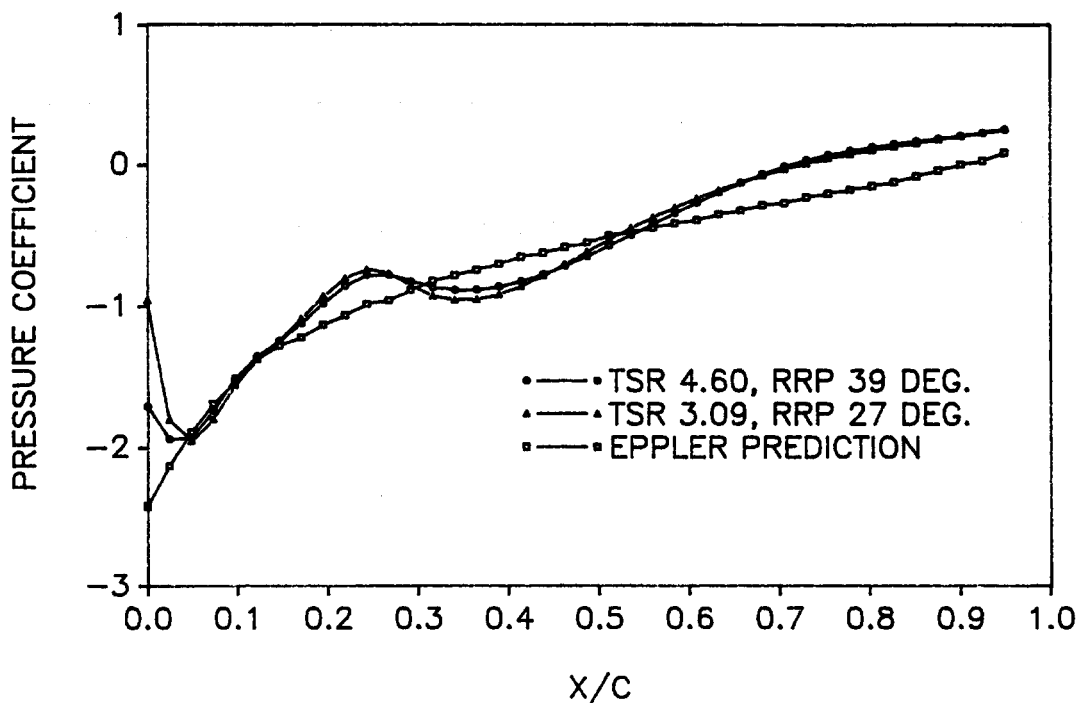


Figure 10b. Pressure Distribution Inner Surface:
Angle of Attack 6 Degrees.

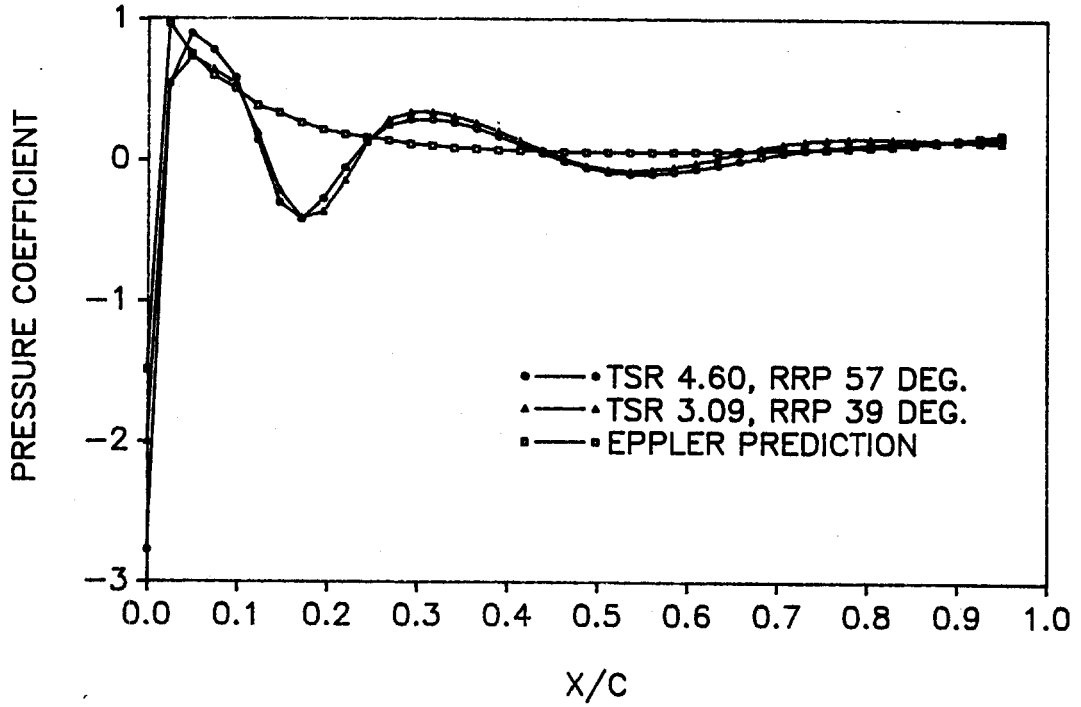


Figure 11a. Pressure Distribution Outer Surface:
Angle of Attack 8 Degrees.

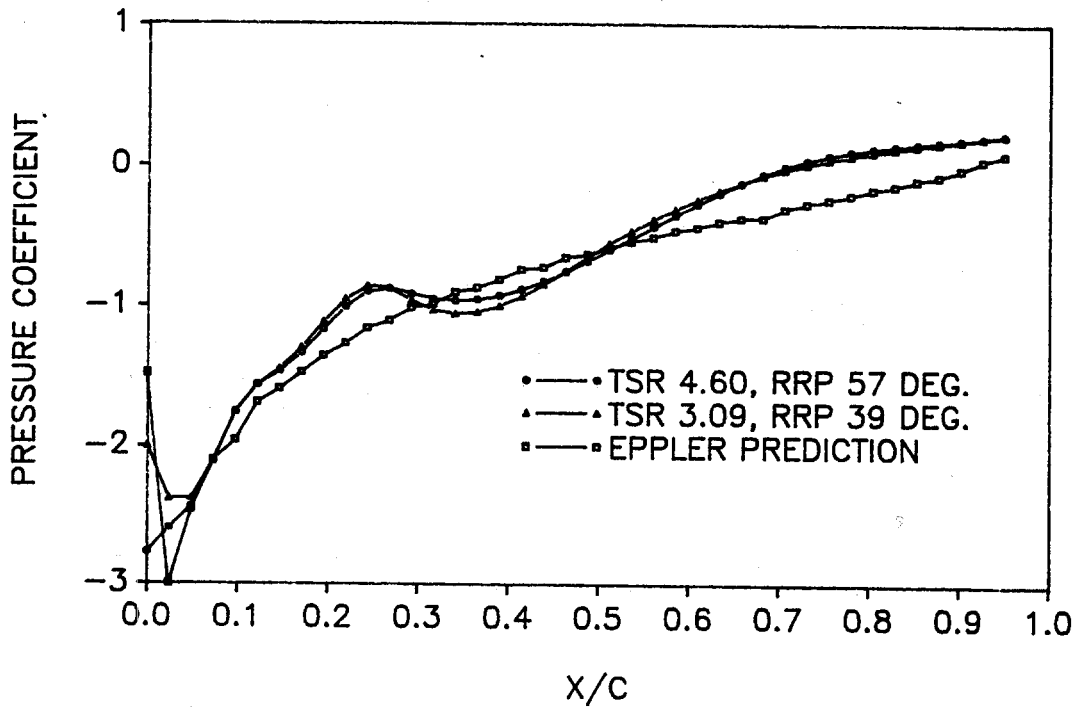


Figure 11b. Pressure Distribution Inner Surface:
Angle of Attack 8 Degrees.

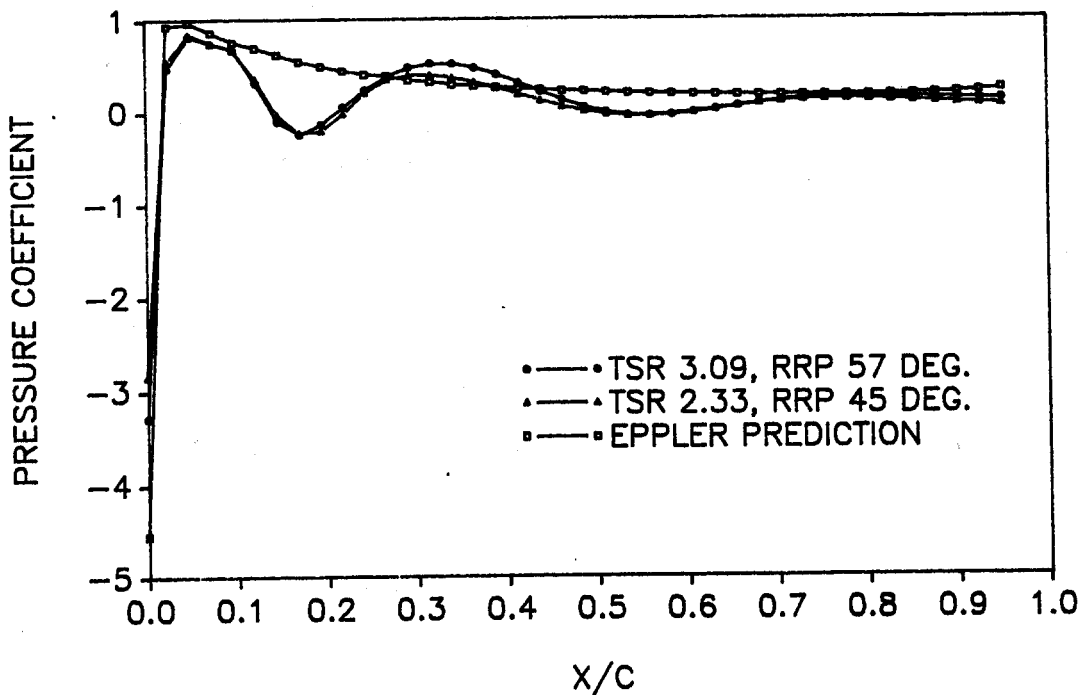


Figure 12a. Pressure Distribution Outer Surface:
Angle of Attack 12 Degrees.

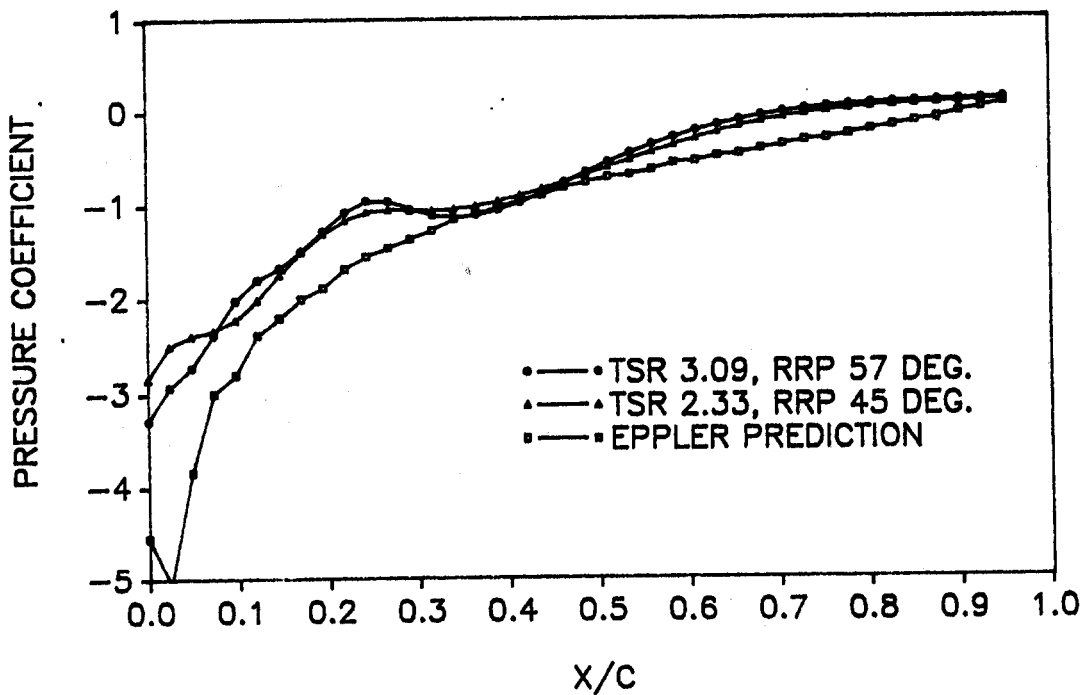


Figure 12b. Pressure Distribution Inner Surface:
Angle of Attack 12 Degrees.

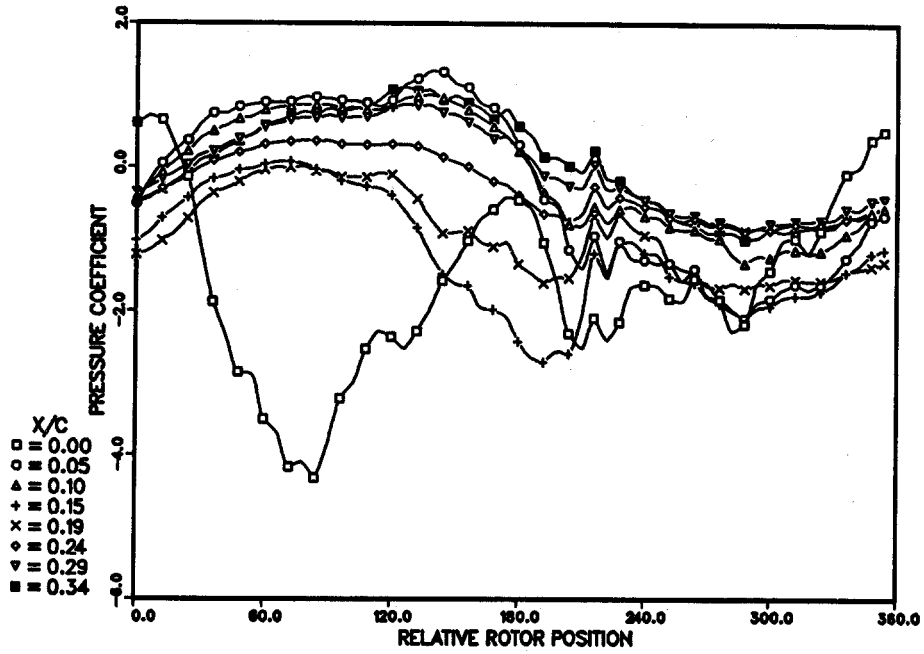


Figure 13a. Pressure Coefficients as a Function of Relative Rotor Position: Outer Surface, Tip-speed ratio 2.33.

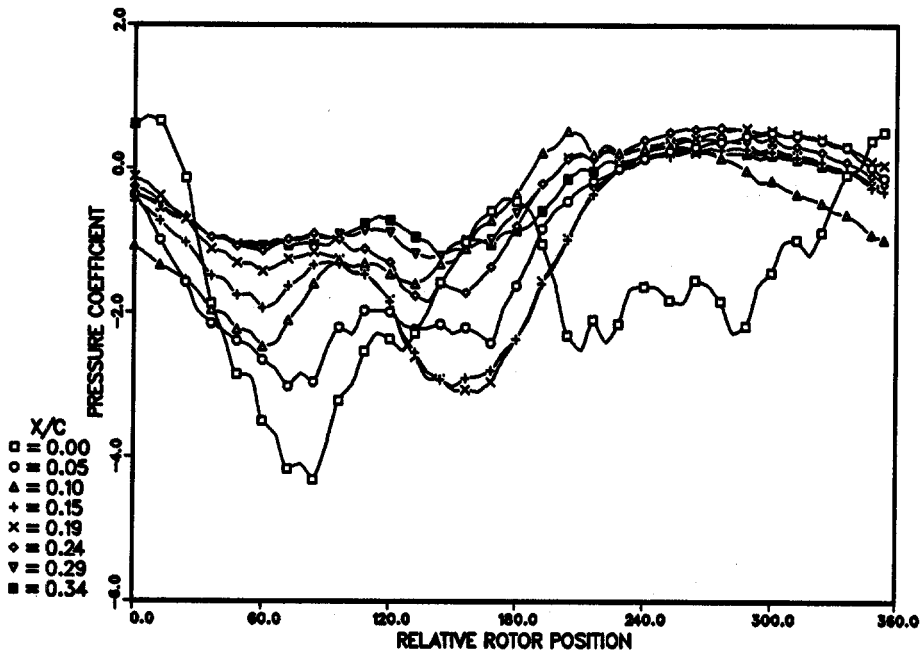


Figure 13b. Pressure Coefficients as a Function of Relative Rotor Position: Inner Surface, Tip-speed ratio 2.33.

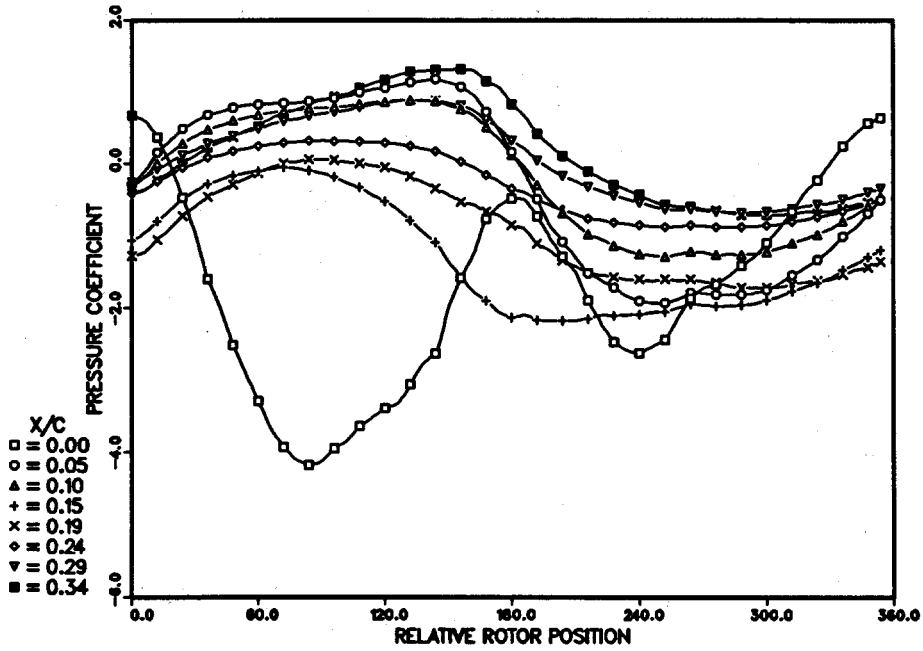


Figure 14a. Pressure Coefficients as a Function of Relative Rotor Position: Outer Surface, Tip-speed ratio 3.09.

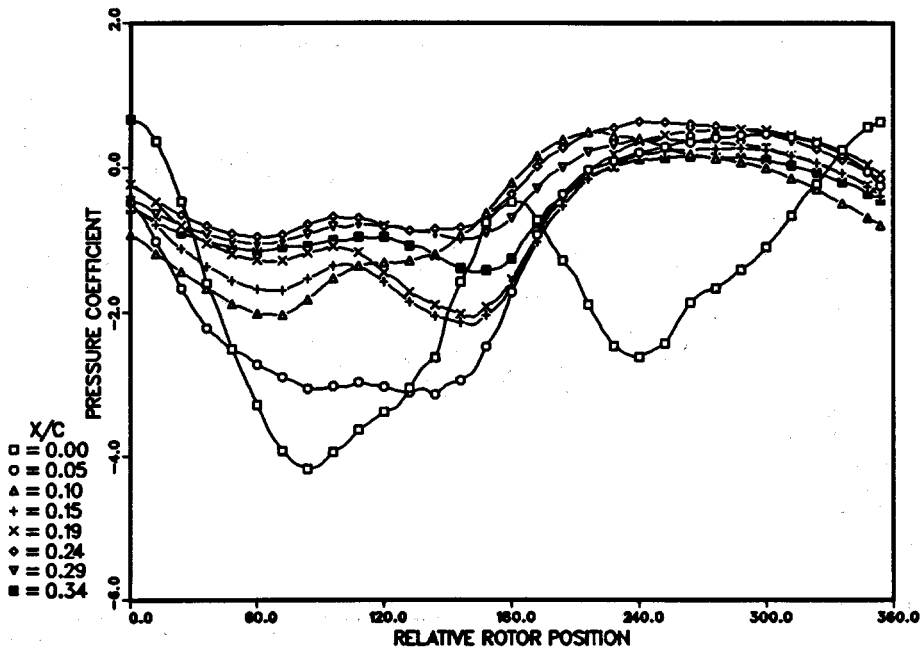


Figure 14b. Pressure Coefficients as a Function of Relative Rotor Position: Inner Surface, Tip-speed ratio 3.09.

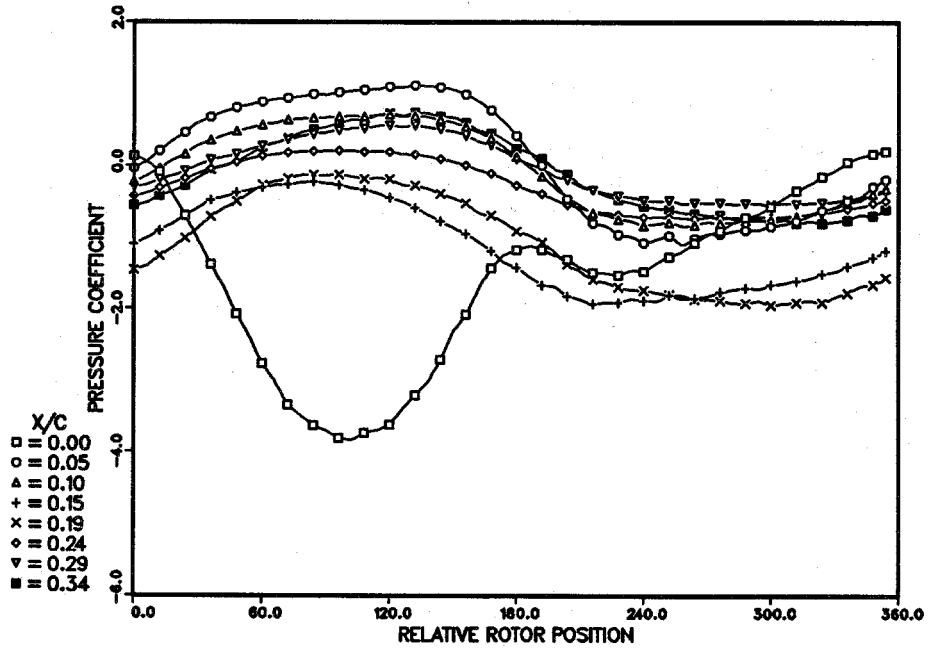


Figure 15a. Pressure Coefficients as a Function of Relative Rotor Position: Outer Surface, Tip-speed ratio 4.60.

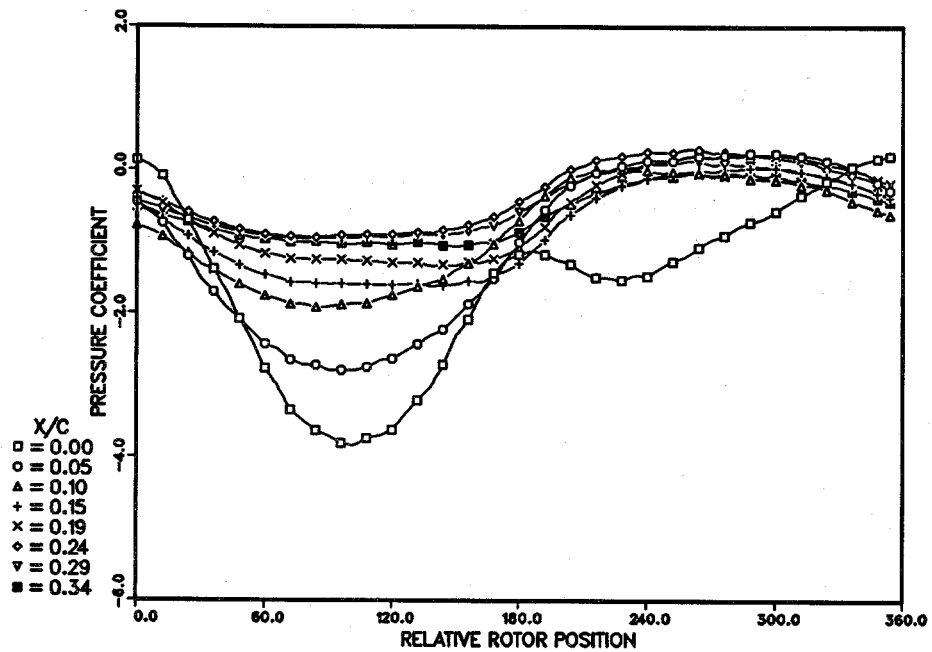


Figure 15b. Pressure Coefficients as a Function of Relative Rotor Position: Inner Surface, Tip-speed ratio 4.60.

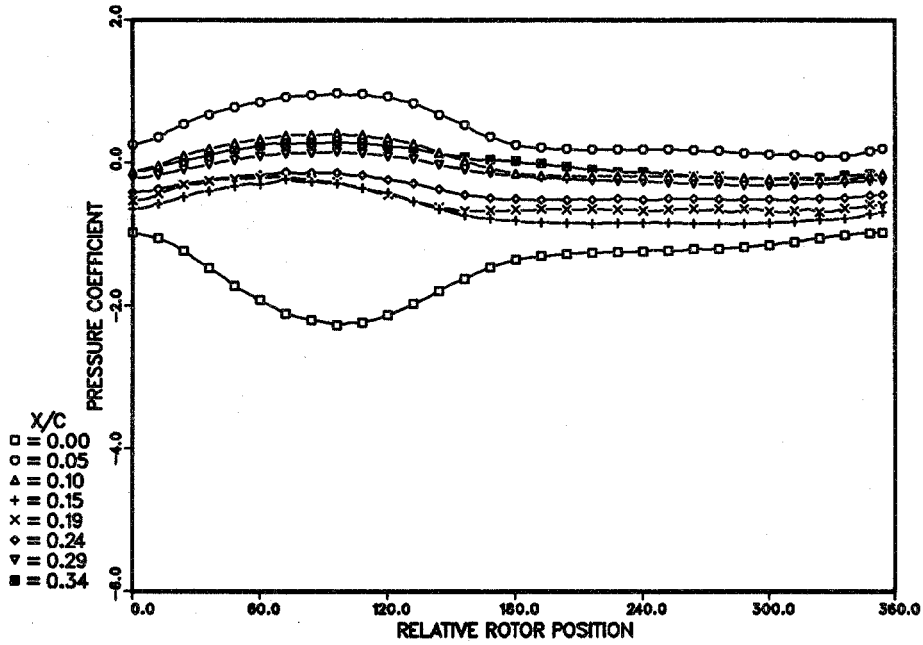


Figure 16a. Pressure Coefficients as a Function of Relative Rotor Position: Outer Surface, Tip-speed ratio 8.92.

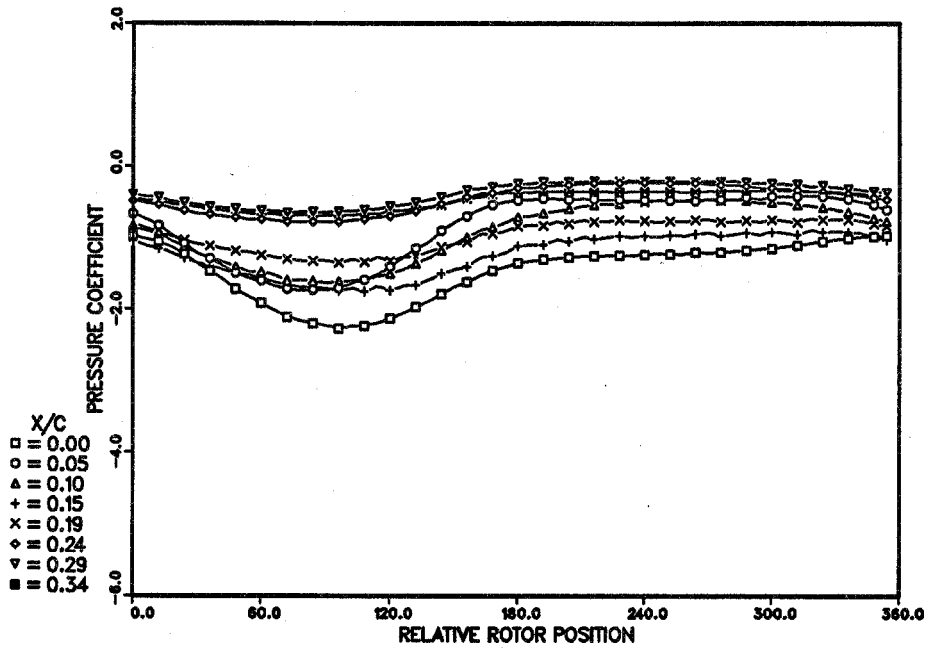


Figure 16b. Pressure Coefficients as a Function of Relative Rotor Position: Inner Surface, Tip-speed ratio 8.92.

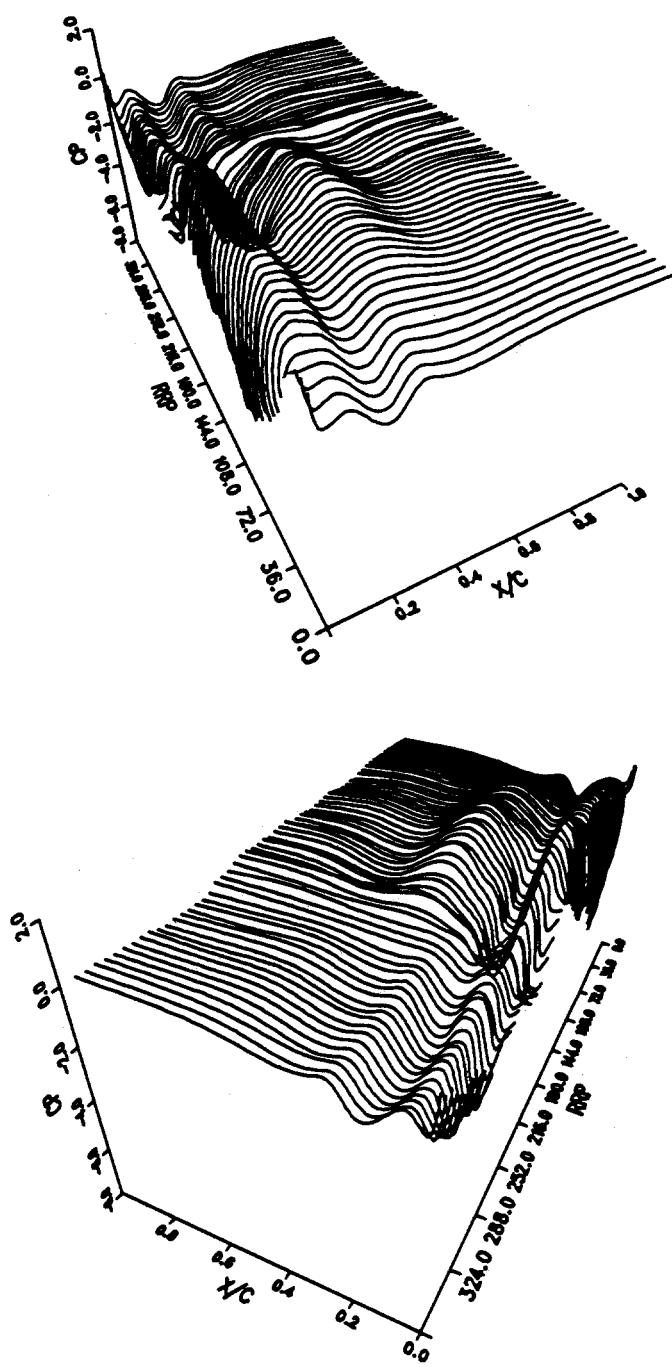


Figure 17a. Surface Plot Pressure Coefficients
Outer Surface, Tip-speed ratio 2.33.

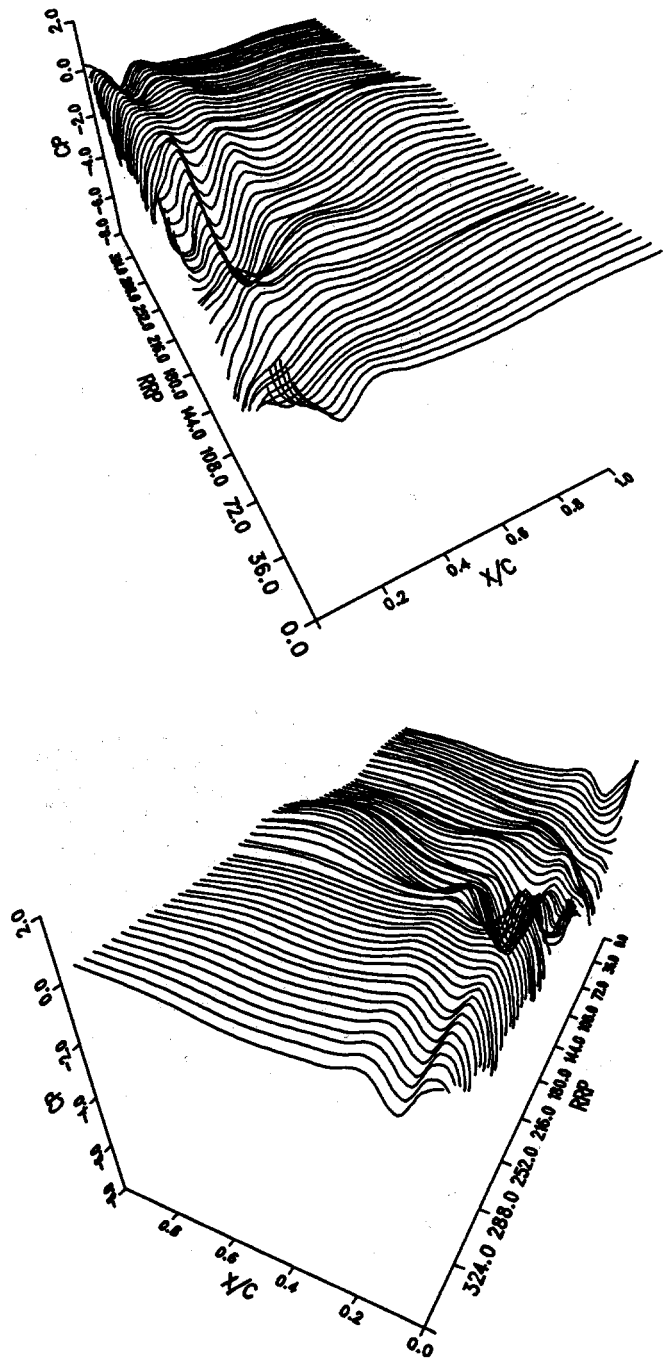


Figure 17b. Surface Plot Pressure Coefficients:
 Inner Surface, Tip-speed ratio 2.33.

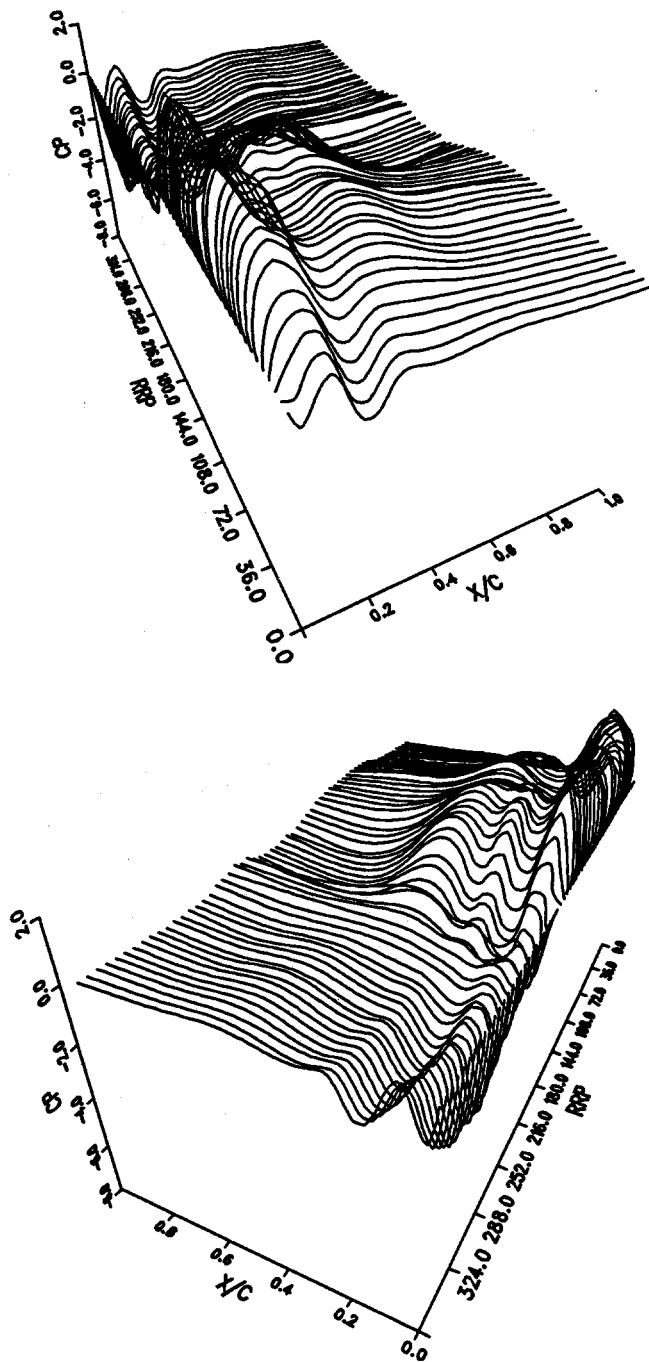


Figure 17c. Surface Plot Pressure Coefficients:
Net Force, Tip-speed ratio 2.33.

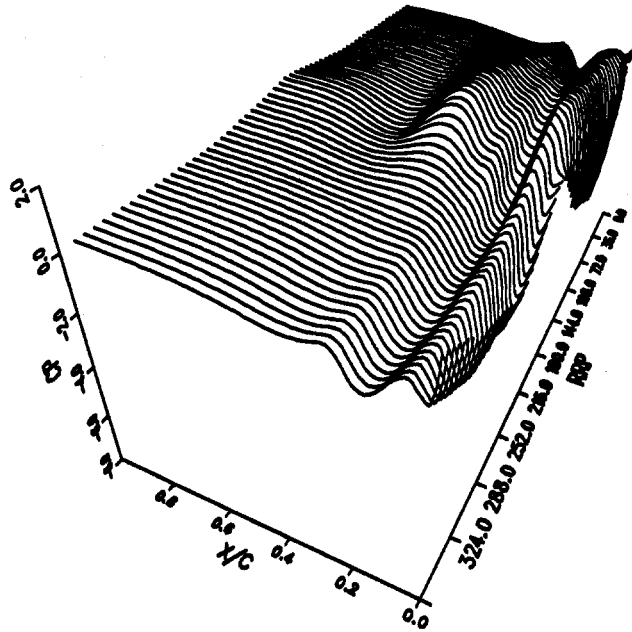
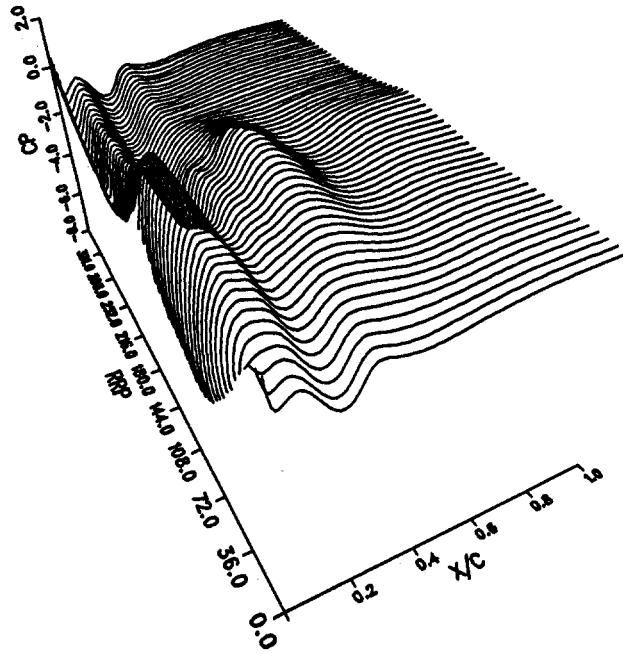


Figure 18a. Surface Plot Pressure Coefficients:
Outer Surface, Tip-speed ratio 3.09.

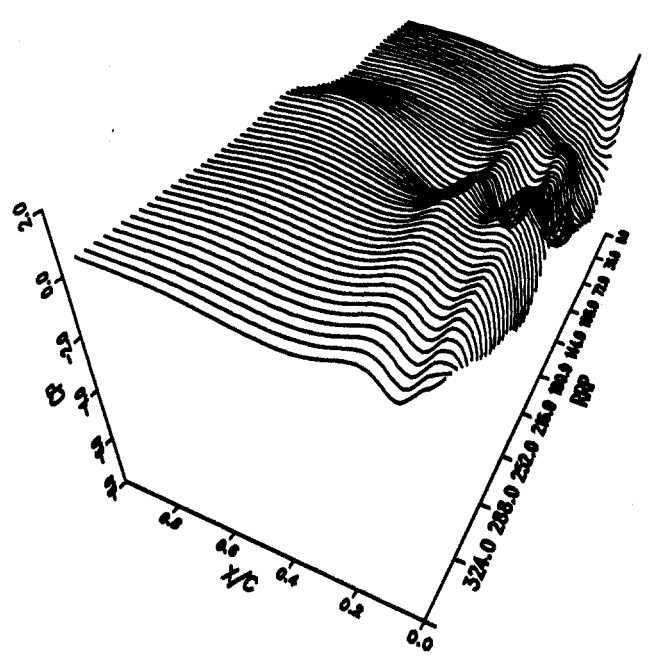
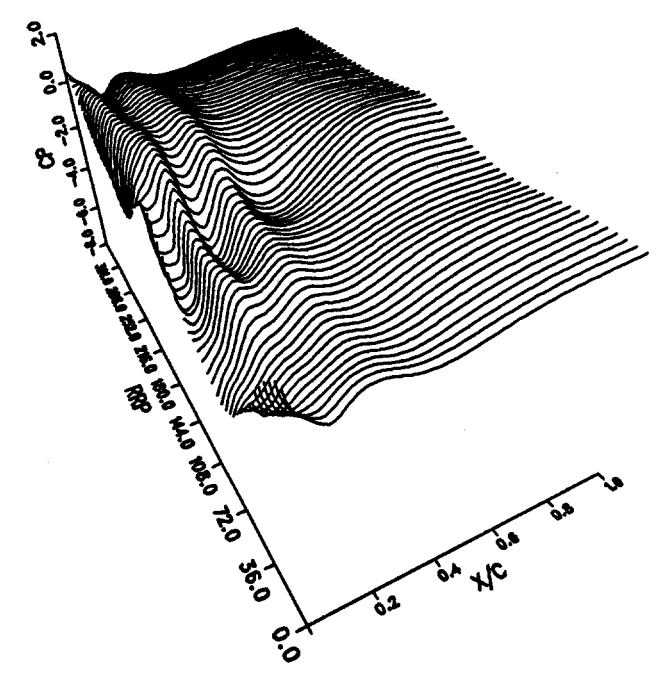


Figure 18b. Surface Plot Pressure Coefficients:
Inner Surface, Tip-speed ratio 3.09.

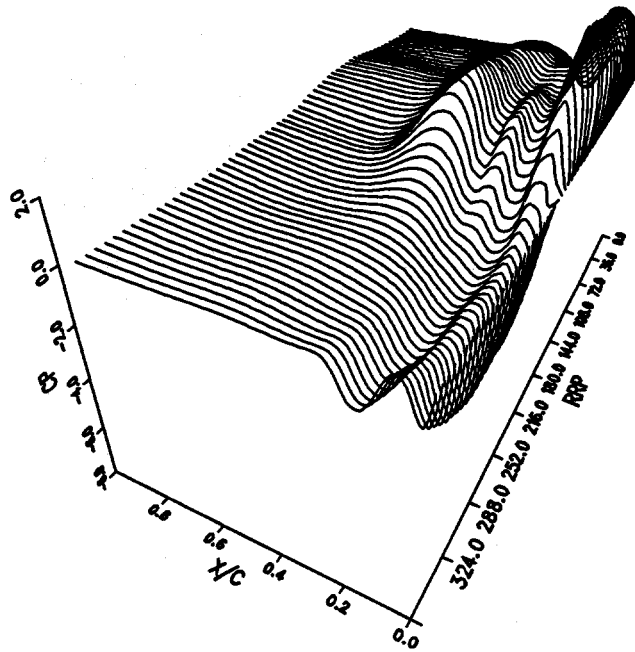
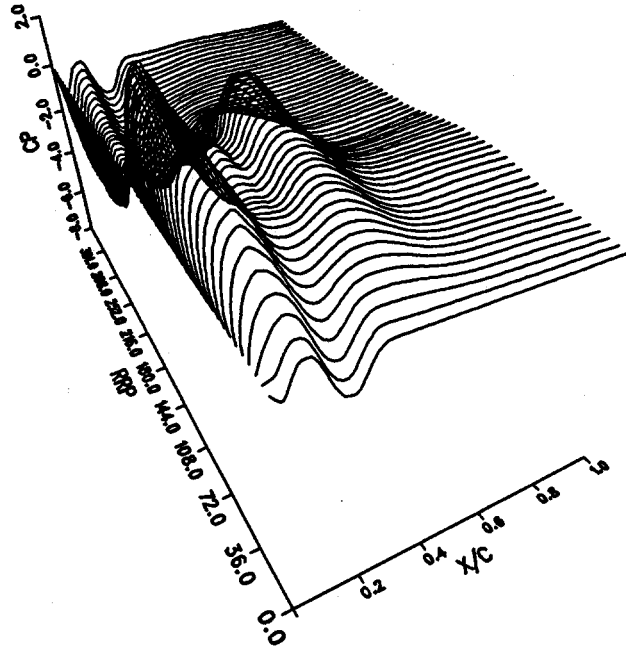


Figure 18c. Surface Plot Pressure Coefficients:
Net Force, Tip-speed ratio 3.09.

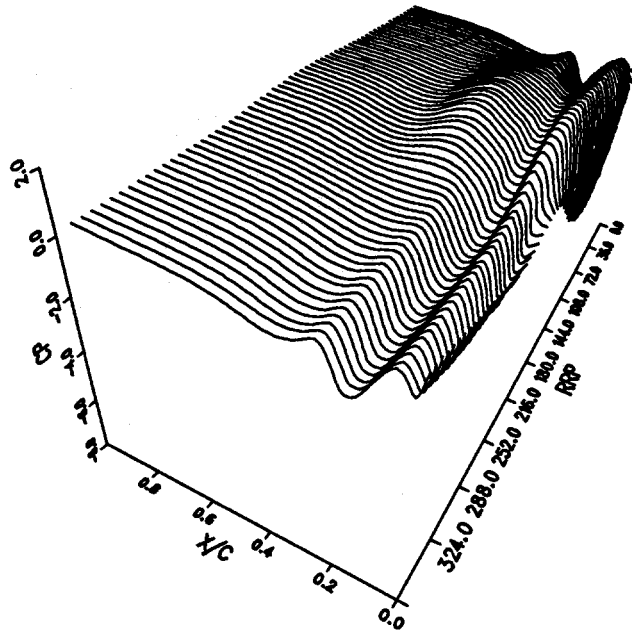
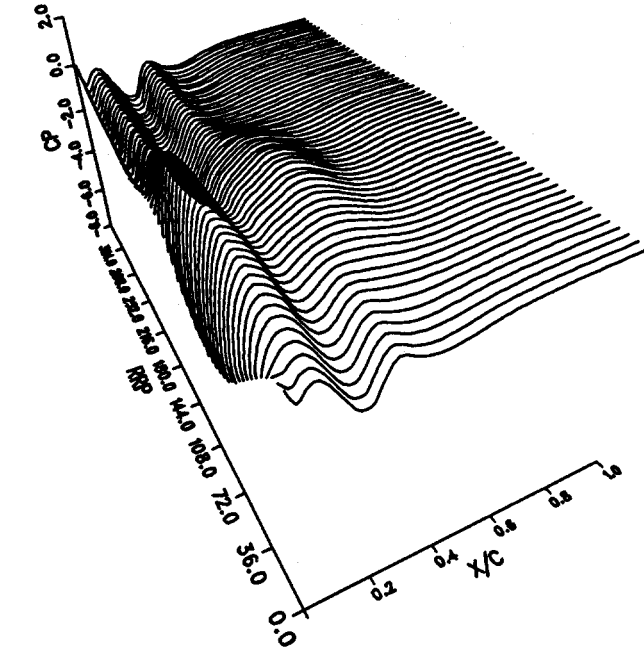


Figure 19a. Surface Plot Pressure Coefficients:
Outer Surface, Tip-speed ratio 4.60.

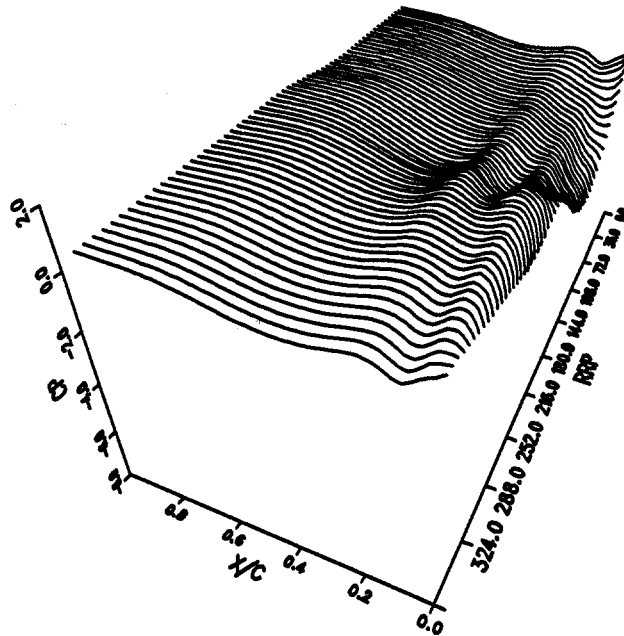
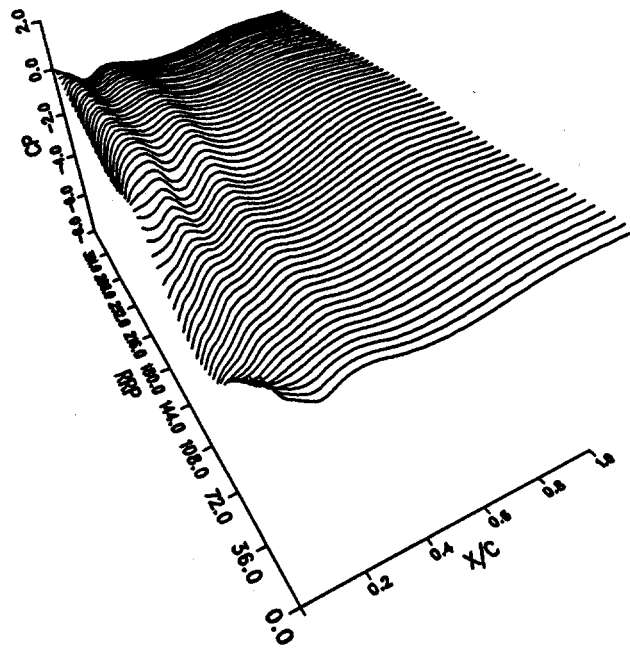


Figure 19b. Surface Plot Pressure Coefficients:
Inner Surface, Tip-speed ratio 4.60.

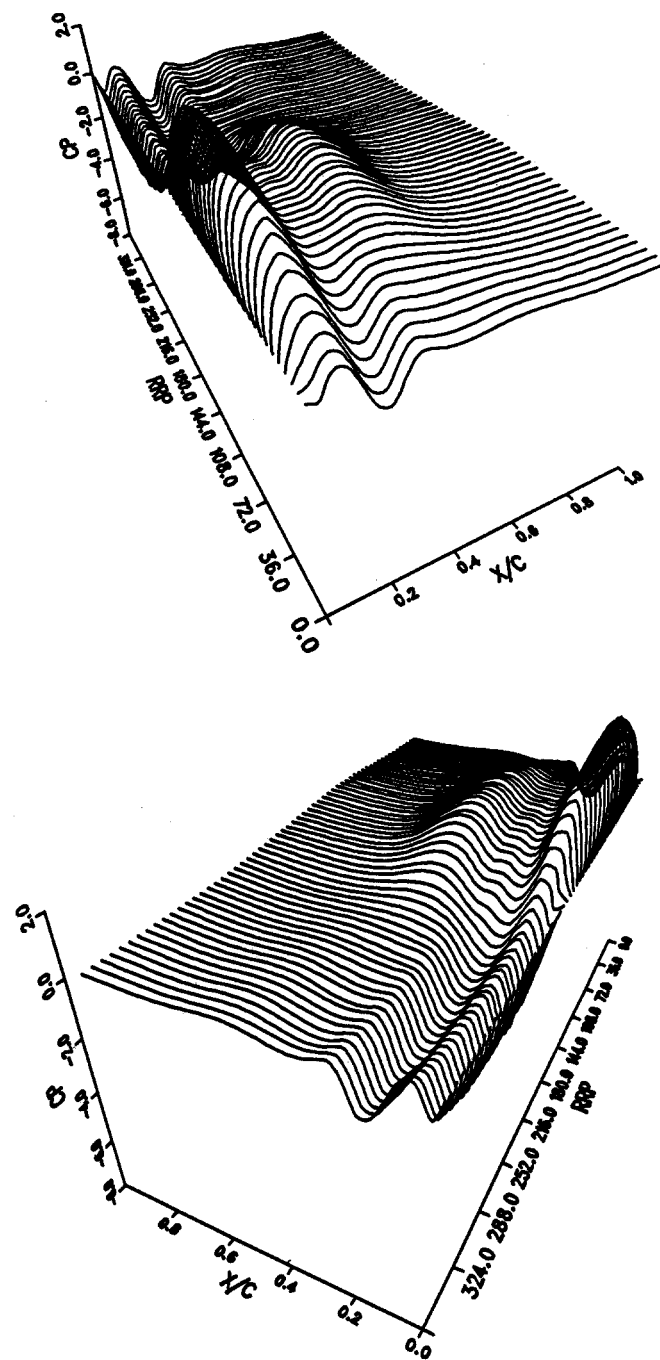


Figure 19c. Surface Plot Pressure Coefficients:
Net Force, Tip-speed ratio 4.60.

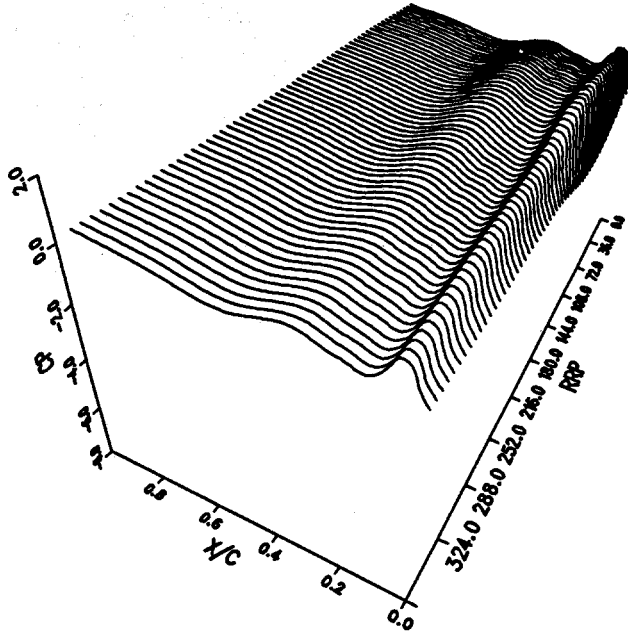
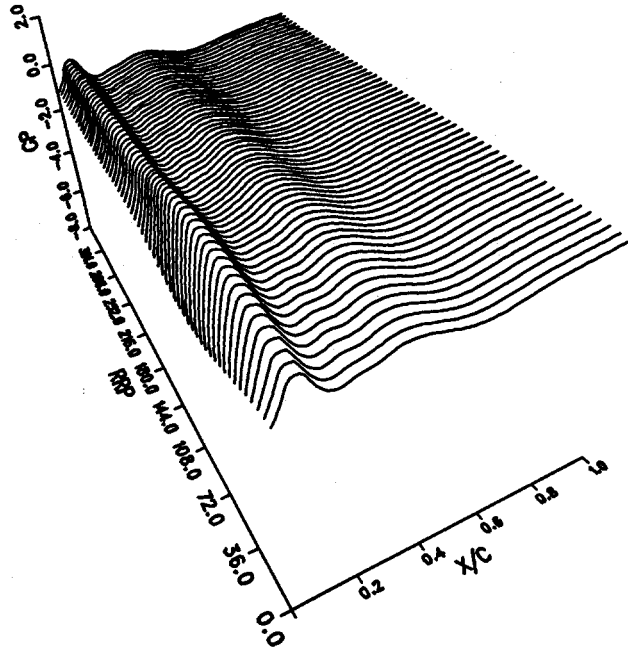


Figure 20a. Surface Plot Pressure Coefficients:
Outer Surface, Tip-speed ratio 8.92.

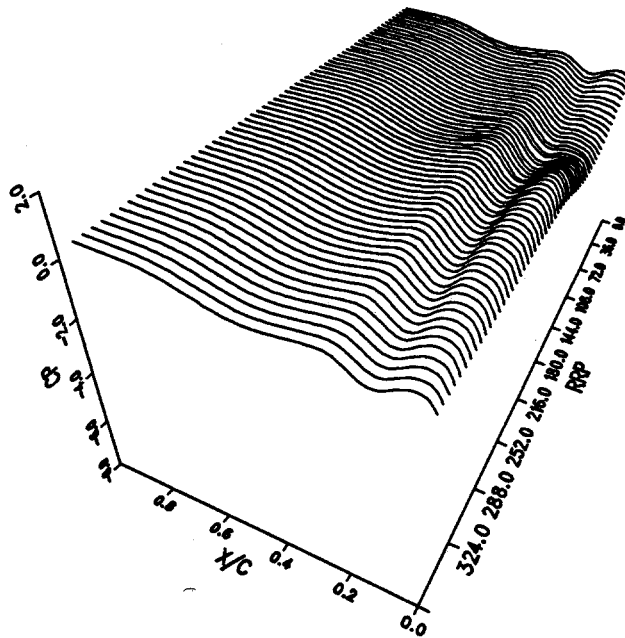
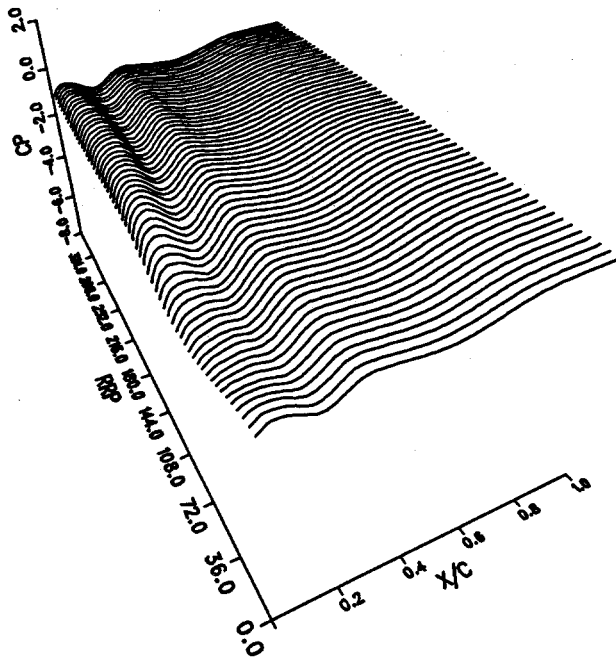


Figure 20b. Surface Plot Pressure Coefficients:
Inner Surface, Tip-speed ratio 8.92.

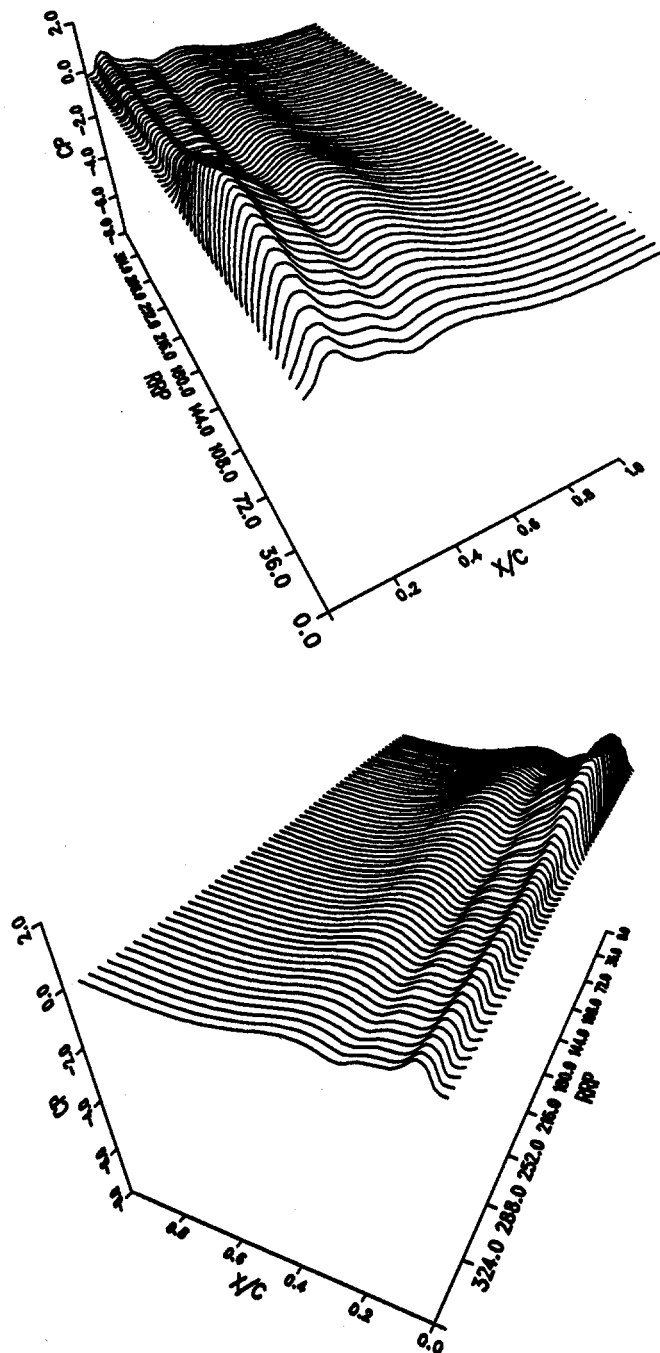


Figure 20c. Surface Plot Pressure Coefficients:
 Net Force, Tip-speed-ratio 8.92.

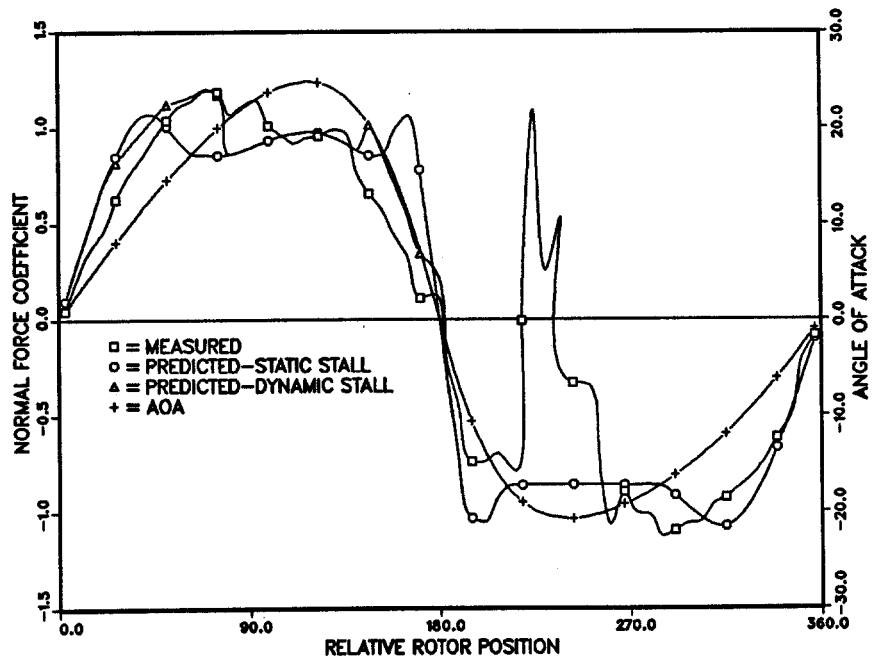


Figure 21. Normal Force Coefficients: Tip-speed ratio 2.20.

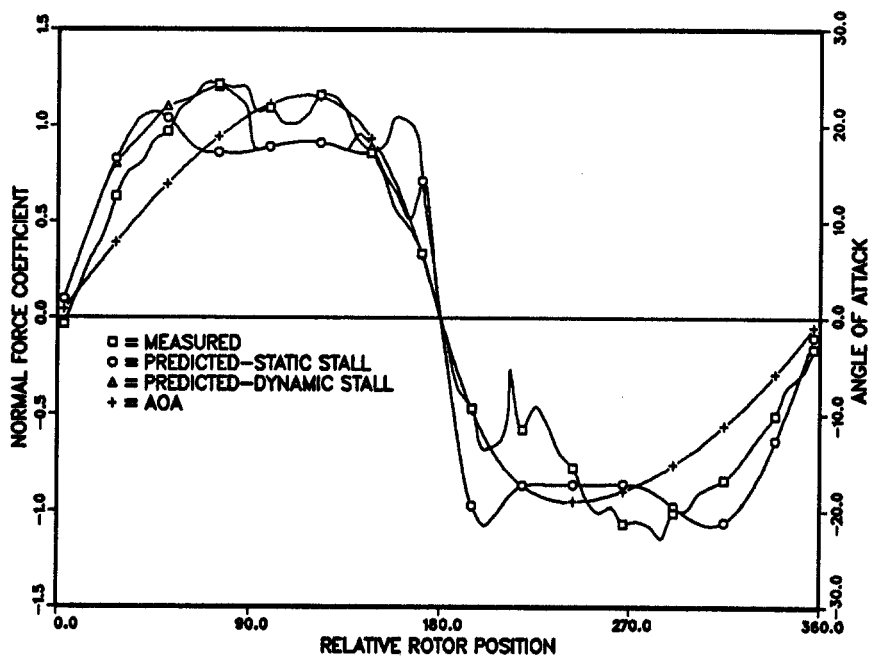


Figure 22. Normal Force Coefficients: Tip-speed ratio 2.33.

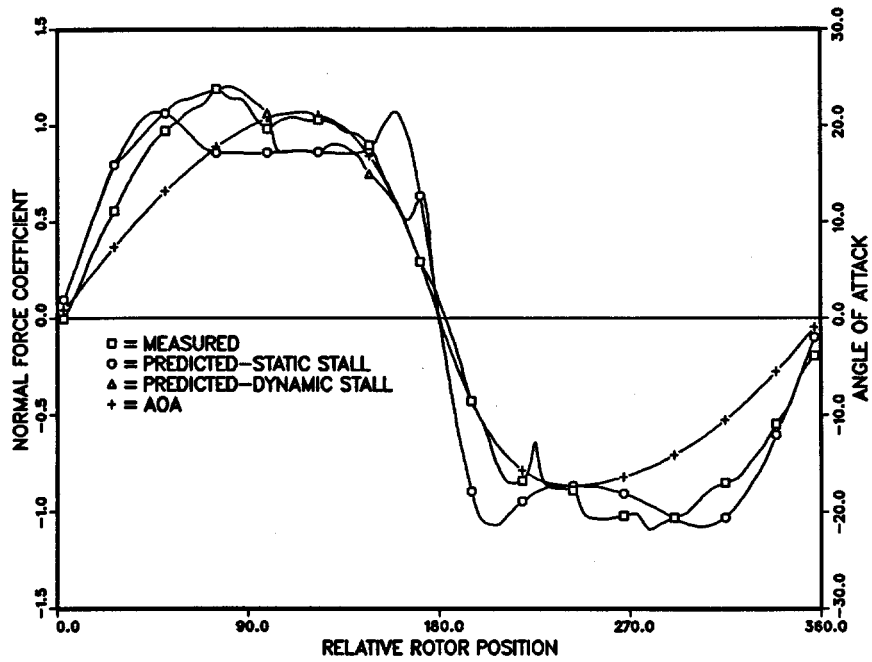


Figure 23. Normal Force Coefficients: Tip-speed ratio 2.49.

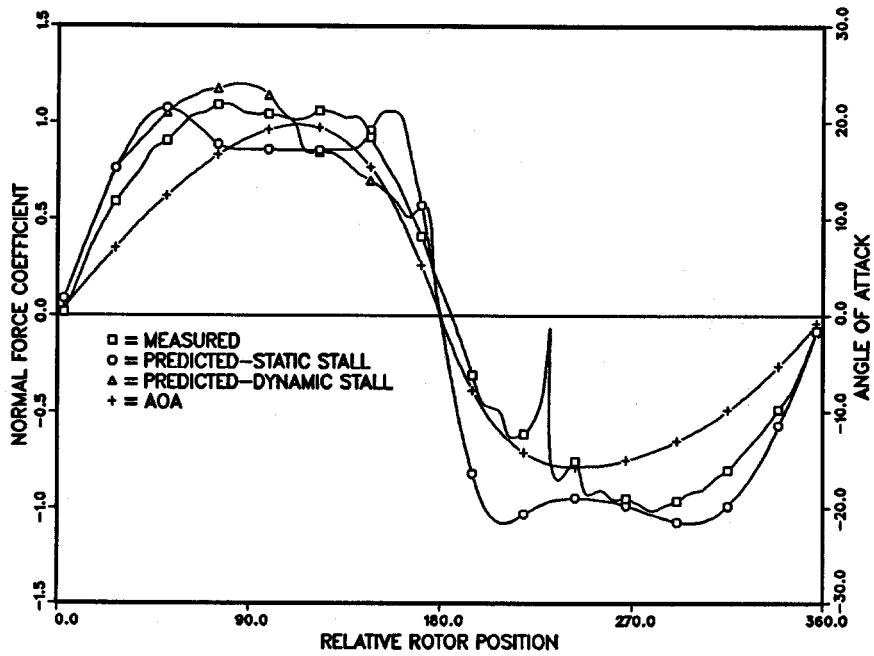


Figure 24. Normal Force Coefficients: Tip-speed ratio 2.66.

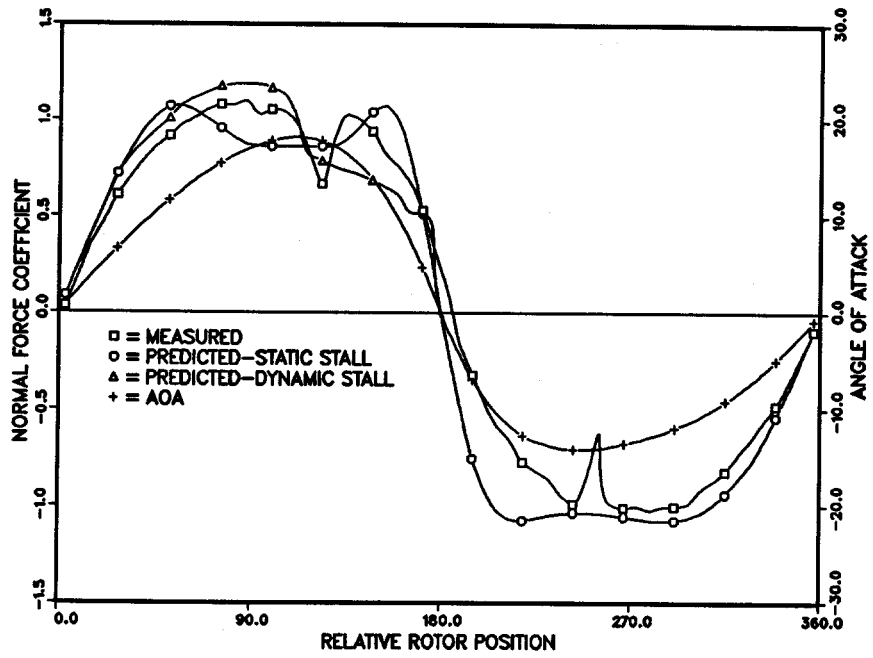


Figure 25. Normal Force Coefficients: Tip-speed ratio 2.86.

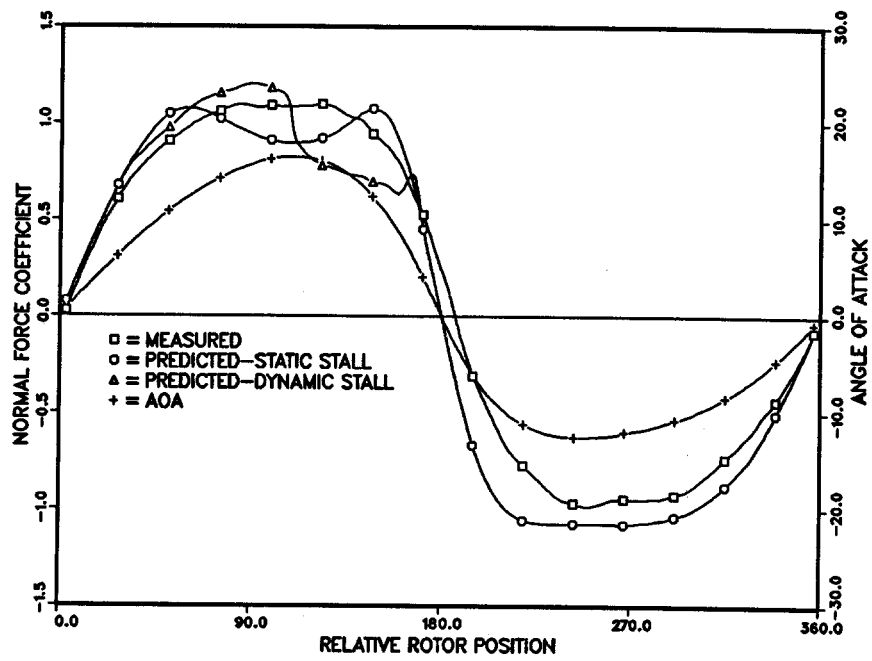


Figure 26. Normal Force Coefficients: Tip-speed ratio 3.09.

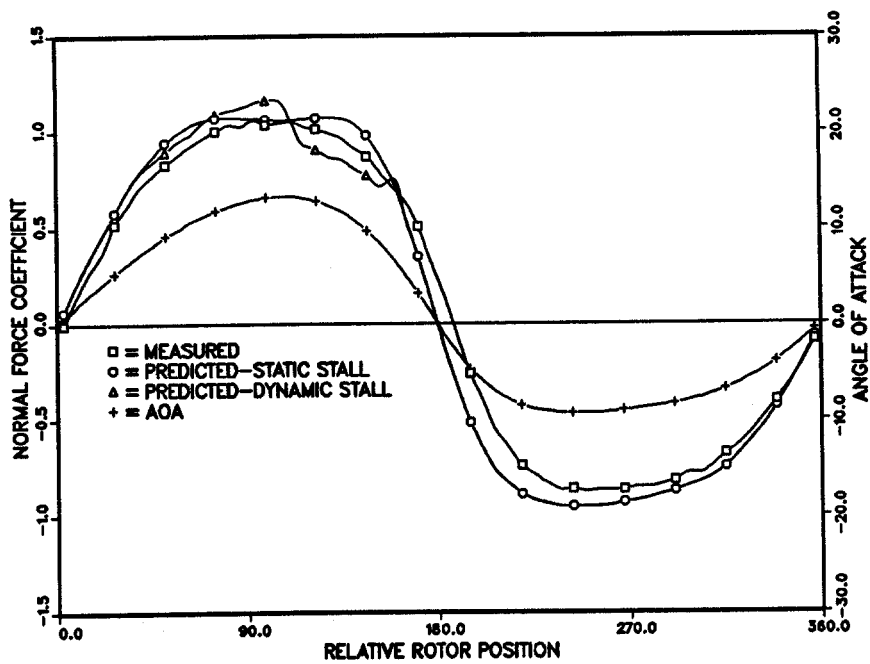


Figure 27. Normal Force Coefficients: Tip-speed ratio 3.70.

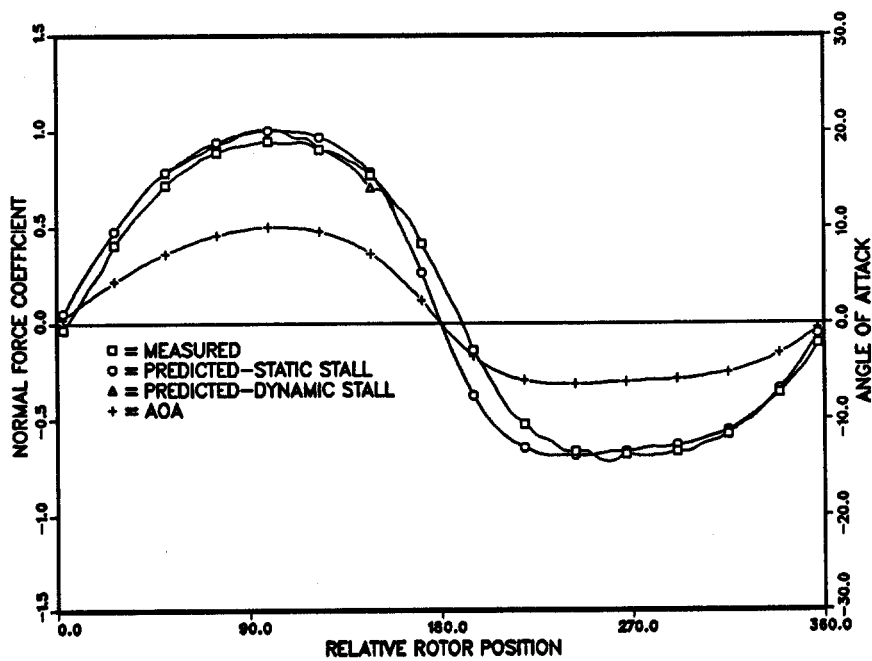


Figure 28. Normal Force Coefficients: Tip-speed ratio 4.60.

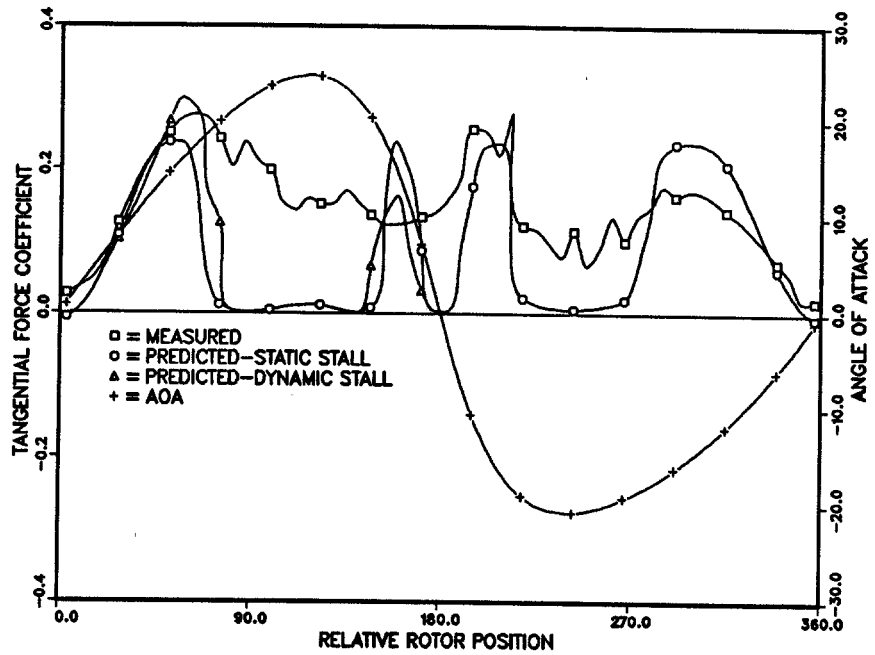


Figure 29. Tangential Force Coefficients: Tip-speed ratio 2.20.

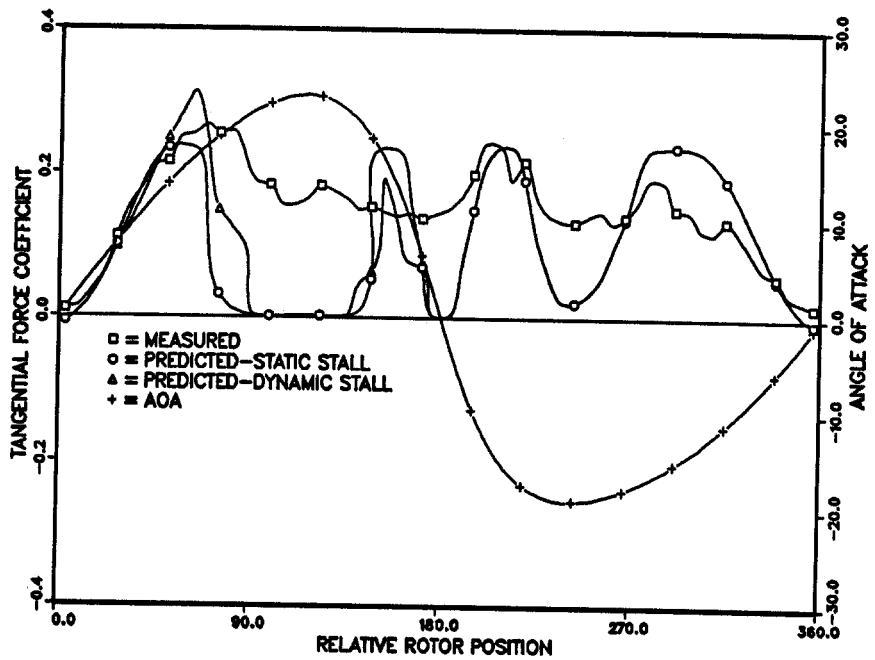


Figure 30. Tangential Force Coefficients: Tip-speed ratio 2.33.

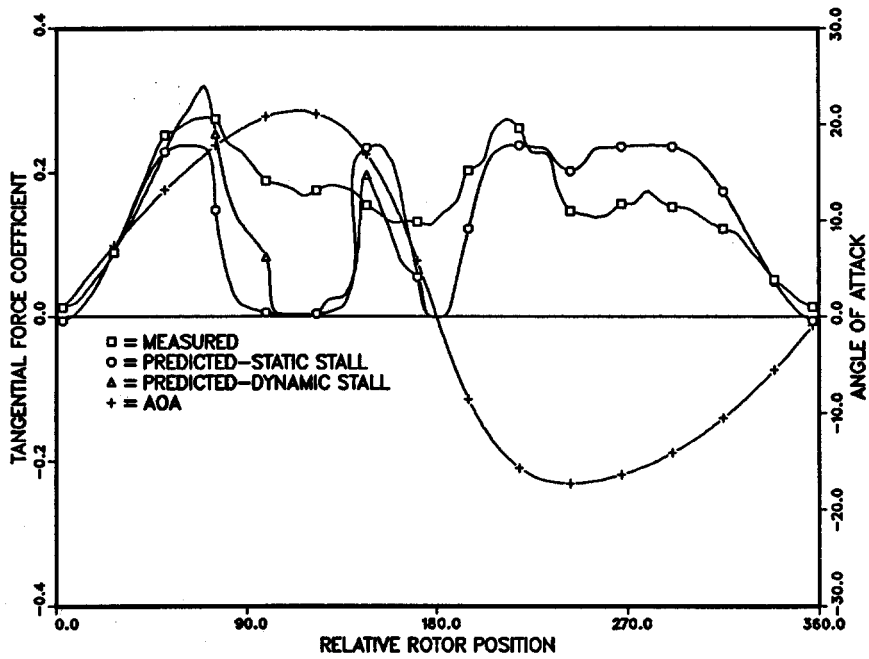


Figure 31. Tangential Force Coefficients: Tip-speed ratio 2.49.

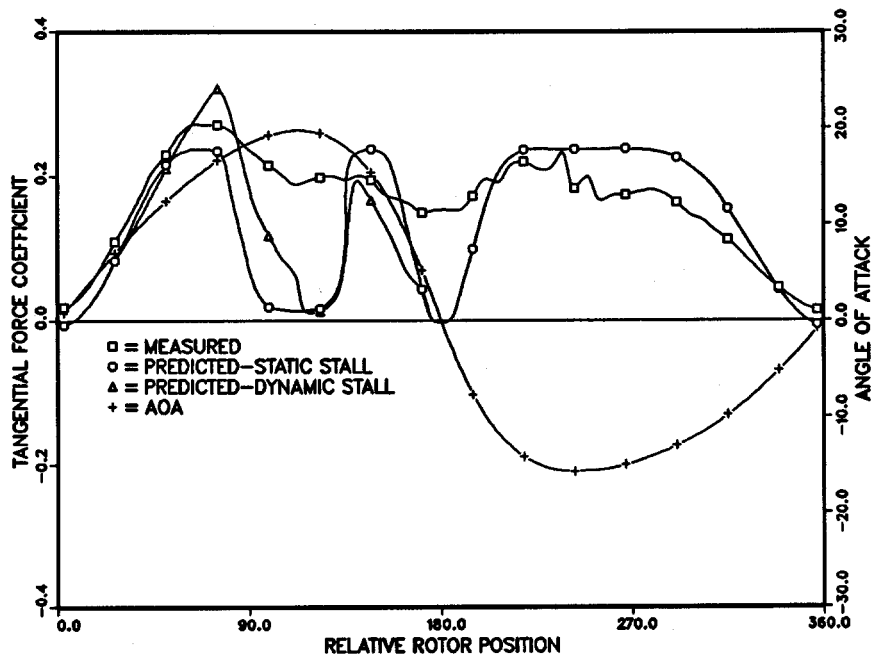


Figure 32. Tangential Force Coefficients: Tip-speed ratio 2.66.

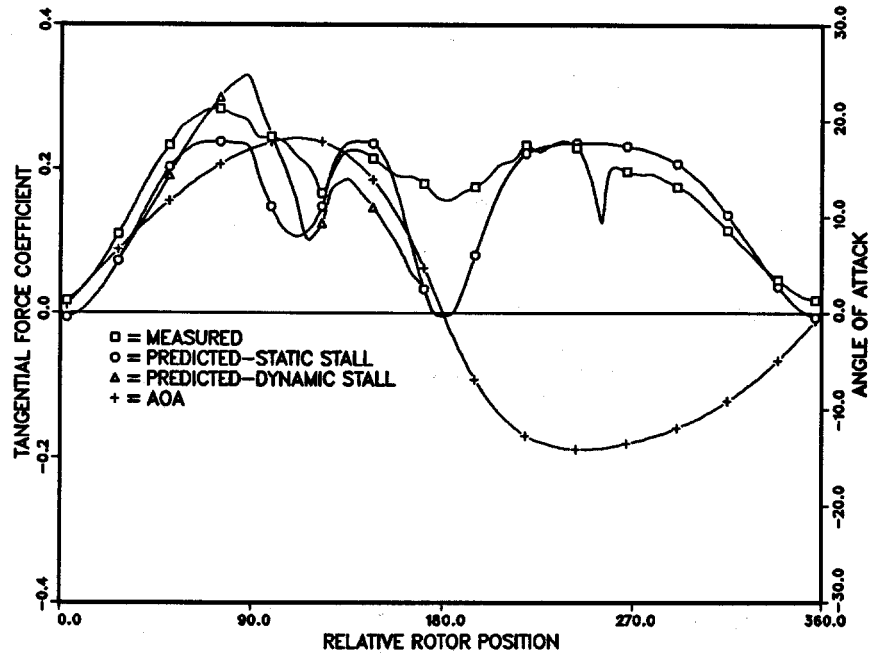


Figure 33. Tangential Force Coefficients: Tip-speed ratio 2.86.

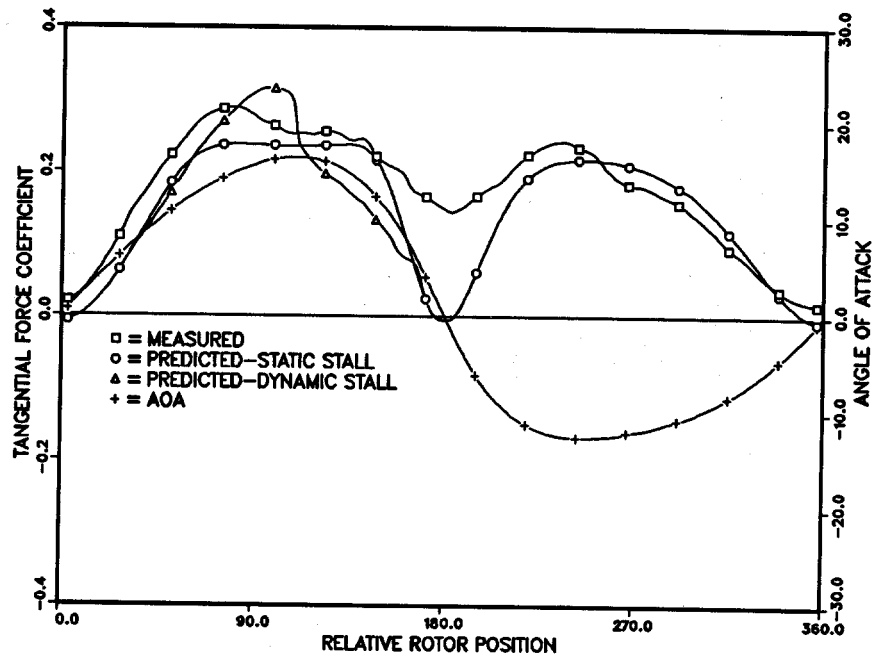


Figure 34. Tangential Force Coefficients: Tip-speed ratio 3.09.

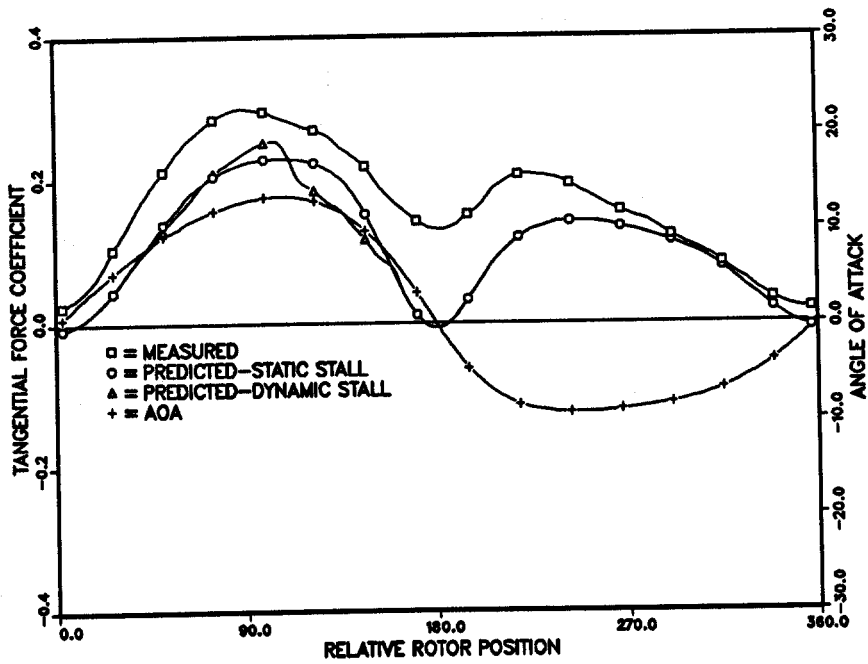


Figure 35. Tangential Force Coefficients: Tip-speed ratio 3.70.

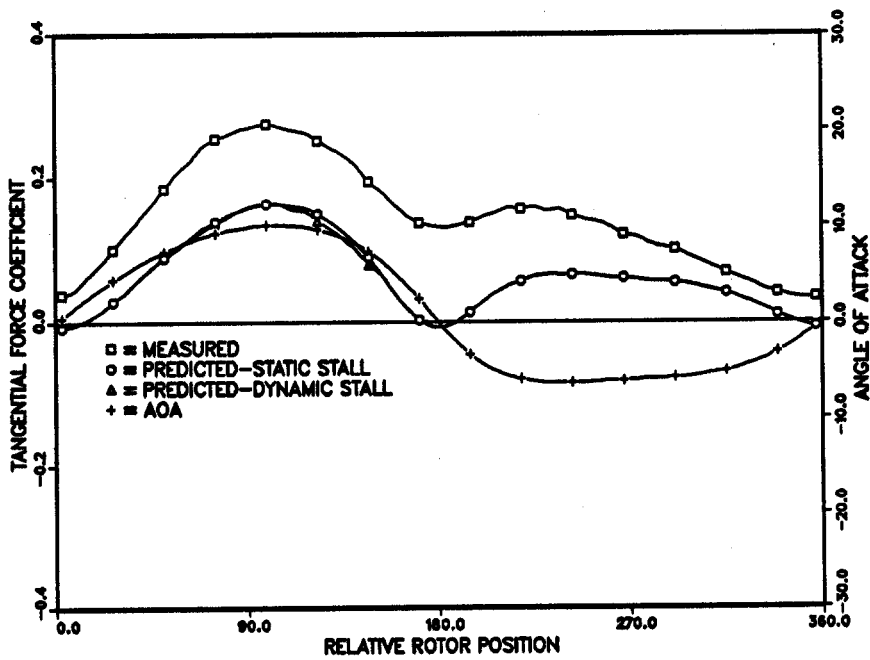


Figure 36. Tangential Force Coefficients: Tip-speed ratio 4.60

DISTRIBUTION:

Advanced Alternative Energy
Solutions
Attn: Ugur Ortabasi
5673 W. Las Positas Boulevard
Suite 205
P.O. Box 5246
Pleasanton, CA

Alcoa Technical Center (5)
Aluminum Company of America
Attn: D. K. Ai
J. T. Huang
J. R. Jombock
M. Klingensmith
J. L. Prohaska
Alcoa Center, PA 15069

Alternative Sources of Energy
Attn: L. Stoiaken
Milaca, MN 56353

Amarillo College
Attn: E. Gilmore
Amarillo, TX 79100

The American Wind Energy Association
1730 N. Lynn Street, #610
Arlington, VA 22209

Roger J. Austin
Hydro-LIFT Systems
125 Catron Drive
Reno, NV 89512

Dr. A. S. Barker
Trinity Western
7600 Glover Road
Langley, BC
CANADA V3A 4R9

Battelle-Pacific Northwest
Laboratory
Attn: L. Wendell
P.O. Box 999
Richland, WA 99352

Bechtel Group, Inc.
Attn: B. Lessley
P.O. Box 3965
San Francisco, CA 94119

Dr. George Bergeles
Dept. of Mechanical Engineering
National Technical University
42, Patission Street
Athens, GREECE

Ir. Jos Beurskens
Programme Manager for
Renewable Energies
Netherlands Energy Research
Foundation ECN
Westerduinweg 3
P.O. Box 1
1755 ZG Petten (NH)
The Netherlands

Bonneville Power Administration
Attn: N. Butler
P.O. Box 3621
Portland, OR 97208

Canadian Standards Association
Attn: T. Watson
178 Rexdale Blvd.
Rexdale, Ontario, M9W 1R3
CANADA

Monique Carpentier
Energy, Mines and Resources
Renewable Energy Branch
460 O'Connor St.
Ottawa, Ontario
CANADA K1A 0E4

Professor V. A. L. Chateau
School of Engineering
University of Auckland
Private Bag
Auckland, NEW ZEALAND

W. H. Cherry
4547 Province Line Road
Princeton, NJ 08540

Colorado State University
Dept. of Civil Engineering
Attn: R. N. Meroney
Fort Collins, CO 80521

Commonwealth Electric Co.
Attn: D. W. Dunham
Box 368
Vineyard Haven, MA 02568

M. M. Curvin
11169 Loop Road
Soddy Daisy, TN 37379

Alcir de Faro Orlando
Pontificia Universidade Catolica-
PUC/Rj
Mechanical Engineering Department
R. Marques de S. Vicente 225
Rio de Janeiro, BRAZIL

Department of Economic Planning
and Development
Barrett Building
Attn: G. N. Monsson
Cheyenne, WY 82002

Beatrice de Saint Louvent
Etablissement d'Etudes et
de Recherches Meteorologiques
77 Rue de Servas
92106 Boulogne-Billancourt Cedex
FRANCE

Otto de Vries
National Aerospace Laboratory
Anthony Fokkerweg 2
Amsterdam 1017
THE NETHERLANDS

DOE/ALO/ETWMD
Attn: G. P. Tennyson
Albuquerque, NM 87115

DOE/ALO
Energy Technology Liaison Office
NGD
Attn: Capt. J. L. Hanson, USAF
Albuquerque, NM 87115

DOE Headquarters (5)
Wind/Oceans Technologies Division
Attn: L. J. Rogers
P. R. Goldman
1000 Independence Avenue
Washington, DC 20585

J. B. Dragt
Nederlands Energy Research
Foundation
(E.C.N.)
Physics Department
Westerduinweg 3 Petten (NH)
THE NETHERLANDS

Electric Power Research Institute
Attn: J. R. Birk
E. A. DeMeo
3412 Hillview Avenue
Palo Alto, CA 94304

George Elliot, Manager
National Wind Turbine Centre
Department of Trade and Industry
National Engineering Laboratory
East Kilbride
Glasgow G75 0QU
Scotland

John Ereaux
RR No. 2
Woodbridge, Ontario L4L 1A6
CANADA

Dr. Norman E. Farb
10705 Providence Drive
Villa Park, CA 92667

Fayette Manufacturing Corporation
Attn: W. Thompson
P.O. Box 1149
Tracy, CA 95378-1149

FloWind Corporation
Attn: L. Schienbein
1183 Quarry Lane
Pleasanton, CA 94566

A. D. Garrad
Garrad Hasson
10 Northampton Square
London EC1M 5PA
UNITED KINGDOM

H. Gerardin
Mechanical Engineering Department
Faculty of Sciences & Engineering
Universite Laval-Quebec, G1K 7P4
CANADA

Dr. I. J. Graham
Southern University
Dept. of Mechanical Engineering
P.O. Box 9445
Baton Rouge, LA 70813-9445

R. T. Griffiths
University College of Swansea
Dept. of Mechanical Engineering
Singleton Park
Swansea, SA2 8PP
UNITED KINGDOM

Helion, Inc.
Attn: J. Park, President
Box 445
Brownsville, CA 95919

Indal Technologies, Inc.
Attn: V. Lacey
3570 Hawkestone Road
Mississauga, Ontario
CANADA L5C 2V8

Institut de Recherche d'Hydro-Quebec
Attn: Bernard Masse
1800, Montee Ste-Julie
Varenes, Quebec, JOL 2P.O.
CANADA

Iowa State University
Agricultural Engineering
Attn: L. H. Soderholm
Room 213
Ames, IA 50010

K. Jackson
Dynamic Design
123 C Street
Davis, CA 95616

M. Jackson
McAllester Financial
1816 Summit
W. Lafayette, IN 47906

Leif G. Johansen
Vice President of Operations
Cannon Energy Corporation
P.O. Box 1457
Tehachapi, CA 93561

KW Control Systems, Inc.
Attn: R. H. Klein
RD#4, Box 914C
South Plank Road
Middletown, NY 10940

Kaiser Aluminum and Chemical
Sales, Inc.
Attn: A. A. Hagman
14200 Cottage Grove Avenue
Dolton, IL 60419

Kaiser Aluminum and Chemical
Sales, Inc.
Attn: D. D. Doerr
6177 Sunol Blvd.
P.O. Box 877
Pleasanton, CA 94566

Kansas State University
Electrical Engineering Department
Attn: Dr. G. L. Johnson
Manhattan, KS 66506

R. E. Kelland
The College of Trades & Technology
P.O. Box 1693
Prince Philip Drive
St. John's, Newfoundland, A1C 5P7
CANADA

Kinetics Group, Inc.
Attn: J. Sladky, Jr.
P.O. Box 1071
Mercer Island, WA 98040

L. K. Liljergren
120 East Penn Street
San Dimas, CA 91773

L. Liljidahl
Building 005, Room 304
Barc-West
Beltsville, MD 20705

Olle Ljungstrom
FFA, The Aeronautical Research
Institute
Box 11021
S-16111 Bromma, SWEDEN

Robert Lynette
R. Lynette & Assoc., Inc.
15042 NE 40th Street
Suite 206
Redmond, WA 98052

David Malcolm
Lavalin Engineers, Inc.
Atria North - Phase 2
2235 Sheppard Avenue East
Willowdale, Ontario M25 5A6
CANADA

Massachusetts Institute of
Technology
Attn: Professor N. D. Ham
W. L. Harris, Aero/Astro
Dept.
77 Massachusetts Avenue
Cambridge, MA 02139

H. S. Matsuda
Composite Materials Laboratory
Pioneering R&D Laboratories
Toray Industries, Inc.
Sonoyama, Otsu, Shiga, JAPAN 520

Brian McNiff
Engineering Consulting Services
55 Brattle Street
So. Berwick, ME 03908

Michigan State University
Division of Engineering Research
Attn: O. Krauss
East Lansing, MI 48825

Napier College of Commerce
and Technology
Tutor Librarian,
Technology Faculty
Colinton Road
Edinburgh, EH10 5DT
ENGLAND

National Rural Electric
Cooperative Assn.
Attn: Wilson Prichett, III
1800 Massachusetts Avenue, NW
Washington, DC 20036

Natural Power, Inc.
Attn: Leander Nichols
New Boston, NH 03070

New Mexico Engineering
Research Institute (2)
Attn: G. G. Leigh
D. Morrison
Campus P.O. Box 25
Albuquerque, NM 87131

Ohio State University
Aeronautical & Astronautical Dept.
Attn: Professor G. Gregorek
2300 West Case Road
Columbus, OH 43220

Oklahoma State University
Mechanical Engineering Dept.
Attn: D. K. McLaughlin
Stillwater, OK 76074

Oregon State University
Mechanical Engineering Dept.
Attn: R. E. Wilson
Corvallis, OR 97331

Debby Oscar
Massachusetts Institute of
Technology
77 Massachusetts Ave.
Room 1-303
Cambridge, MA 02139

Pacific Gas & Electric Co.
Attn: T. Hillesland
J. J. Iannucci
W. J. Steeley
3400 Crow Canyon Road
San Ramon, CA 94583

Ion Paraschivoiu
Dept. of Mechanical Engineering
Ecole Polytechnique
CP 6079
Succursale A
Montreal, Quebec
CANADA H3C 3A7

Jacques Plante
Shawinigan Consultants, Inc.
620 Dorchester Blvd. West
Montreal, Quebec
CANADA H3B 1N8

Public Service Co. of New Hampshire
Attn: D. L. C. Frederick
1000 Elm Street
Manchester, NH 03105

Public Service Co. of New Mexico
Attn: M. Lechner
P.O. Box 2267
Albuquerque, NM 87103

Dr. R. Ganesh Rajagopalan,
Asst. Prof.
Aerospace Engineering Department
Iowa State University
404 Town Engineering Bldg.
Ames, IA 50011

R. Rangi (2)
Low Speed Aerodynamics Laboratory
NRC-National Aeronautical
Establishment
Montreal Road
Ottawa, Ontario, K1A 0R6
CANADA

RANN, Inc.
Attn: A. J. Eggers, Jr.
260 Sheridan Ave., Suite 414
Palo Alto, CA 94306

Mr. Bent Rasmussen
Overgade 14
DK-7000 Fredericia
DENMARK

Markus G. Real, President
Alpha Real Ag
Feldeggstrasse 89
CH 8008 Zurich
Switzerland

The Resources Agency
Department of Water Resources
Energy Division
Attn: R. G. Ferreira
P.O. Box 388
Sacramento, CA 95802

Reynolds Metals Company
Mill Products Division
Attn: G. E. Lennox
6601 West Broad Street
Richmond, VA 23261

R. G. Richards
Atlantic Wind Test Site
P.O. Box 189
Tignish P.E.I., COB 2B0
CANADA

Riso National Laboratory
Attn: Troels Friis Pedersen
Helge Petersen
Peter Hauge Madsen
Postbox 49
DK-4000 Roskilde
DENMARK

H. M. Romanowitz, P. E.
Oak Creek Energy Systems, Inc.
P.O. Box 469
Tehachapi, CA 93561

Dr. Ing. Hans Ruscheweyh
Institut fur Leichbau
Technische Hochschule Aachen
Wullnerstrasse 7
FEDERAL REPUBLIC OF GERMANY

Gwen Schreiner
Librarian
National Atomic Museum
Albuquerque, NM 87185

Arnan Seginer
Professor of Aerodynamics
Technion-Israel Institute of
Technology
Aeronautical Engineering Dept.
Haifa
ISRAEL

Mr. Farrell Smith Seiler, Editor
Wind Energy News Service
P.O. Box 4008
St. Johnsbury, VT 05819

David Sharpe
Dept. of Aeronautical Engineering
Queen Mary College
Mile End Road
London, E1 4NS
UNITED KINGDOM

Kent Smith
Instituto Tecnológico Costa Rica
Apartado 159 Cartago
COSTA RICA

Solar Energy Research Institute
Attn: R. W. Thresher
1617 Cole Boulevard
Golden, CO 80401

Bent Sorenson
Roskilde University Center
Energy Group, Bldg. 17.2
IMFUFA
P.O. Box 260
DK-400 Roskilde
DENMARK

Peter South
ADECON
6535 Millcreek Dr., Unit 67
Mississauga, Ontario
CANADA L5N 2M2

Southern California Edison
Research & Development Dept.
Room 497
Attn: R. L. Scheffler
P.O. Box 800
Rosemead, CA 91770

G. Stacey
The University of Reading
Department of Engineering
Whiteknights, Reading, RG6 2AY
ENGLAND

Stanford University
Dept. of Aeronautics and
Astronautics Mechanical Engr.
Attn: Holt Ashley
Stanford, CA 94305

Dr. Derek Taylor
Alternative Energy Group
Walton Hall
Open University
Milton Keynes, MK7 6AA
UNITED KINGDOM

Texas Tech University
Mechanical Engineering Dept.
Attn: J. W. Oler
P.O. Box 4289
Lubbock, TX 79409

K. J. Touryan
P.O. Box 713
Indian Hills, CO 80454

Tulane University
Dept. of Mechanical Engineering
Attn: R. G. Watts
New Orleans, LA 70018

J. M. Turner Technologies, Inc.
Attn: Eric N. Hinrichsen
P.O. Box 1058
Schenectady, NY 12301-1058

US WindPower
Attn: W. E. Holley
G. M. McNerney
Suite 3050
400 West Cummings Park
Woburn, MA 01803

USDA
Agricultural Research Service
Southwest Great Plains Research
Center
Attn: Dr. R. N. Clark
Bushland, TX 79012

United Engineers and
Constructors, Inc.
Attn: A. J. Karalis
P.O. Box 8223
Philadelphia, PA 19101

Universal Data Systems
Attn: C. W. Dodd
5000 Bradford Drive
Huntsville, AL 35805

University of California
Institute of Geophysics
and Planetary Physics
Attn: Dr. P. J. Baum
Riverside, CA 92521

University of Colorado
Dept. of Aerospace
Engineering Sciences
Attn: J. D. Fock, Jr.
Boulder, CO 80309

University of Massachusetts
Mechanical and Aerospace
Engineering Dept.
Attn: Dr. D. E. Cromack
Amherst, MA 01003

University of Oklahoma
Aero Engineering Department
Attn: K. Bergey
Norman, OK 73069

University of Sherbrooke
Faculty of Applied Science
Attn: A. Laneville
P. Vittecoq
Sherbrooke, Quebec, J1K 2R1
CANADA

The University of Tennessee
Dept. of Electrical Engineering
Attn: T. W. Reddoch
Knoxville, TN 37916

W. A. Vachon
W. A. Vachon & Associates
P.O. Box 149
Manchester, MA 01944

Dirk Vandenberghe
State Univ. of Ghent
St. Pietersnieuwstraat 41
9000 Ghent
BELGIUM

Washington & Lee University
Attn: Dr. R. E. Akins
P.O. Box 735
Lexington, VA 24450

Washington State University
Dept. of Electrical Engineering
Attn: F. K. Bechtel
Pullman, WA 99163

West Texas State University
Government Depository Library
Number 613
Canyon, TX 79015

West Texas State University
Department of Physics
Attn: V. Nelson
P.O. Box 248
Canyon, TX 79016

West Virginia University
Dept. of Aero Engineering
Attn: R. Walters
1062 Kountz Avenue
Morgantown, WV 26505

D. Westlind
Central Lincoln People's
Utility District
2129 North Coast Highway
Newport, OR 97365-1795

Wichita State University
Aero Engineering Department (2)
Attn: M. Snyder
W. Wentz
Wichita, KS 67208

Wind Power Digest
Attn: Michael Evans
P.O. Box 700
Bascom, OH 44809

400 R. C. Maydew
1520 L. W. Davison
1522 R. C. Reuter, Jr.
1522 D. W. Lobitz
1522 E. D. Reedy
1523 J. H. Biffle
1524 C. R. Dohrmann
1524 D. R. Martinez
1550 C. W. Peterson
1552 J. H. Strickland
1556 G. F. Homicz
3141 S. A. Landenberger (5)
3151 W. I. Klein (3)
3154-1 C. L. Ward (8)
For DOE/OSTI (Unlimited
Release)
3161 P. S. Wilson
6000 D. L. Hartley
6200 V. L. Dugan
6217 P. C. Klimas
6220 D. G. Schueler
6225 H. M. Dodd (50)
6225 T. D. Ashwill
6225 D. E. Berg
6225 M. E. Ralph
6225 D. C. Reda
6225 M. A. Rumsey
6225 L. L. Schluter
6225 W. A. Stephenson
6225 H. J. Sutherland
6225 P. S. Veers
7544 D. O. Smallwood
7544 T. G. Carne
7544 J. Lauffer
8524 J. A. Wackerly



8232-2/069848



00000001 -



8232-2/069848



00000001 -



8232-2/069848



00000001 -

8524

8524-2